NATIONAL ADVISORY COMMITTEE FOR AERONAUTICS

TECHNICAL NOTE 4341

LOW-SPEED EXPERIMENTAL DETERMINATION OF THE EFFECTS OF LEADING-EDGE RADIUS AND PROFILE THICKNESS ON STATIC AND OSCILLATORY LATERAL STABILITY DERIVATIVES FOR A DELTA WING WITH 60° OF LEADING-EDGE SWEEP

By Herman S. Fletcher

Langley Aeronautical Laboratory
Langley Field, Va.

Washington
July 1958

NATIONAL ADVISORY COMMITTEE FOR AERONAUTI

TECHNICAL NOTE 4341

LOW-SPEED EXPERIMENTAL DETERMINATION OF THE EFFECTS OF LEADING-EDGE RADIUS AND PROFILE THICKNESS ON STATIC AND OSCILLATORY LATERAL STABILITY DERIVATIVES FOR A DELTA WING WITH 60° OF LEADING-EDGE SWEEP

By Herman S. Fletcher

SUMMARY

An investigation was made in the Langley stability tunnel to determine the effects of leading-edge radius and profile thickness on the oscillatory lateral stability derivatives for a series of delta wings with 60° of leading-edge sweep. The wings were oscillated in yaw about their vertical axes.

The results of this investigation indicated that there were noticeable decreases in all the derivatives due to increase in leading-edge radius at angles of attack above approximately 12°. Profile-thickness effects were found to be small for the yawing-moment derivatives; however, the data showed that an increase in profile thickness caused appreciable increases in the combination oscillatory derivatives of rolling moment with respect to yawing velocity and rolling moment with respect to sideslip acceleration as well as large decreases in the effective-dihedral parameter at angles of attack above 8°. The static derivatives of rolling and yawing moment with respect to sideslip C_{l_β} and C_{n_β} showed essentially the same effects of leading-edge radius and profile thickness as the oscillatory derivatives.

INTRODUCTION

Recent oscillation-in-yaw tests of two delta wings with 60° of leading-edge sweep but of different airfoil sections (flat plate and NACA 65A003) have shown significant differences in the magnitudes of the dynamic lateral stability derivatives at angles of attack above approximately 12° for the rolling-moment derivatives and above approximately 20°

for the yawing-moment derivatives (ref. 1). It appears that the differences in magnitude can be attributed partly to the type and degree of flow separation present on the wing (refs. 2 and 3) as affected by, among other variables, the wing leading-edge radius (refs. 4, 5, 6, and 7) and profile thickness. The purpose of this paper, therefore, is to present the results of a systematic investigation of the effects of wing leading-edge radius and profile thickness on the dynamic lateral stability derivatives for a 60° delta wing of aspect ratio 2.31 with modified double-wedge airfoil sections. The model wing was oscillated about a fixed vertical axis relative to the model and, hence, the model motion was a combination of yawing and sideslipping. The stability derivatives measured by this technique are the combination derivatives $C_{n_{r,\omega}} - C_{n_{\dot{\beta},\omega}}$, $C_{l_{r,\omega}} - C_{l_{\dot{\beta},\omega}}$, $C_{n_{\beta,\omega}} + k^2 C_{n_{\dot{r},\omega}}$, and $C_{l_{\beta,\omega}} + k^2 C_{l_{\dot{r},\omega}}$ where the symbols are defined in the following section.

SYMBOLS

The data are presented in the form of standard coefficients of forces and moments referred to the stability system of axes with the origin at the projection on the plane of symmetry of the quarter-chord point of the mean aerodynamic chord. The positive direction of forces, moments, and angular displacements are shown in figure 1.

A	aspect ratio, b^2/S
b	span, ft
c	local wing chord, ft
$\bar{c}$	mean aerodynamic chord, ft
C_{D}'	drag coefficient (approximate), F_{D}'/qs
C_L	lift coefficient, F_L/qs
C_l	rolling-moment coefficient, M_X/qsb
C_m	pitching-moment coefficient, $M_Y/qs\bar{c}$
C_n	yawing-moment coefficient, M_Z/qsb
F_{D}'	drag force, lb (approximate)

F_L lift force, lb

F_Y side force, lb

k reduced-frequency parameter, $\omega b/2V$

M_X rolling moment, ft-lb

M_Y pitching moment, ft-lb

M_Z yawing moment, ft-lb

q dynamic pressure, $\rho V^2/2$, lb/sq ft

r yawing angular velocity

$\dot{r} = \frac{\delta^2\psi}{\partial\tau^2} = \frac{\partial r}{\partial\tau}$

S wing area, sq ft

t wing thickness, percent c

V free-stream velocity, ft/sec

X,Z longitudinal and vertical stability axes, respectively

α angle of attack, deg

β angle of sideslip, radians or deg

$\dot{\beta} = \partial\beta/\partial\tau$

Λ angle of sweep of quarter chord, deg

ρ mass density of air, slugs/cu ft

τ time, sec

ψ angle of yaw, radians or deg

$\dot{\psi} = r = \frac{\partial\psi}{\partial\tau}$

ψ_o amplitude of yaw, radians or deg

ω circular frequency of oscillation, radians/sec

Derivatives:

$$C_{L_\alpha} = \frac{\partial C_L}{\partial \alpha}$$

$$C_{l_\beta} = \frac{\partial C_l}{\partial \beta}$$

$$C_{l_{\dot{\beta}}} = \frac{\partial C_l}{\partial\left(\frac{\dot{\beta} b}{2V}\right)}$$

$$C_{l_r} = \frac{\partial C_l}{\partial\left(\frac{rb}{2V}\right)}$$

$$C_{l_{\dot{r}}} = \frac{\partial C_l}{\partial\left(\frac{\dot{r} b^2}{4V^2}\right)}$$

$$C_{n_\beta} = \frac{\partial C_n}{\partial \beta}$$

$$C_{n_{\dot{\beta}}} = \frac{\partial C_n}{\partial\left(\frac{\dot{\beta} b}{2V}\right)}$$

$$C_{n_r} = \frac{\partial C_n}{\partial\left(\frac{rb}{2V}\right)}$$

$$C_{n_{\dot{r}}} = \frac{\partial C_n}{\partial\left(\frac{\dot{r} b^2}{4V^2}\right)}$$

All the above derivatives are nondimensionalized in this paper per radian (1/radian). Leading-edge radius is given in percent local chord.

The symbol ω following the subscript of a derivative denotes the oscillatory derivative.

APPARATUS AND MODELS

Oscillation and Recording Apparatus

The models were oscillated by the apparatus shown schematically in figure 2, which consisted of a motor-driven flywheel, connecting rod, crank arm, and model-support strut.

Recording of data was accomplished by means of the equipment described in the appendix of reference 8. Briefly, the rolling and yawing moments acting on the model during oscillation were measured by means of resistance-type strain gages mounted on the oscillating strut to which the model was attached. The strain-gage signals were modified by a sine-cosine resolver driven by the oscillating mechanism so that the output signals were proportional to the in-phase and out-of-phase moments. These signals were read visually on a highly damped direct-current meter, and the aerodynamic coefficients were obtained by multiplying the meter readings by the appropriate constants.

MODELS

The models tested were the six lightweight 60° delta wings shown in figures 3 and 4. Four of the wings were 3 percent thick and had leading-edge radii of 0, 0.115, 0.791, and 1.582 percent wing chord. The two additional wings had leading-edge radii of 0.791 percent wing chord and were 5 and 8 percent thick. All trailing-edge radii were zero. The leading and trailing one-third of each wing was beveled as shown in figure 3. The wing construction was a combination of balsa wood core covered with laminated fiber glass to a depth of 0.016 inch and reinforced with hardwood strips at the mounting point. A balsa canopy served to streamline the protrusion of the strain-gage balance above the upper surface of the 3-percent-thick models.

TESTS AND CORRECTIONS

Tests

The static and oscillatory tests were conducted in the 6- by 6-foot test section of the Langley stability tunnel at a dynamic pressure of 24.9 pounds per square foot, which corresponds to a Mach number of 0.13 and a Reynolds number based on the wing mean aerodynamic chord of approximately 1.6×10^6.

The static tests made to determine the static longitudinal stability characteristics of the six model wings utilized the six-component electromechanical balance system. The approximate angle-of-attack range for the static tests was from -4° to 32° in 4° increments. Additional static tests utilizing the strain-gage balance used in the oscillation tests were made to determine the static rolling and yawing moments for angles of sideslip of 2°, 4°, 6°, 8°, and 10°.

The oscillatory tests were made at frequencies of 0.5, 1.0, 2.0, and 3.3 cycles per second, which correspond to values of the reduced-frequency parameter k of 0.033, 0.066, 0.132, and 0.218. The complete frequency range was covered for an amplitude ψ_o of $\pm 6^\circ$. Amplitudes of $\pm 2^\circ$ and $\pm 10^\circ$ were used at frequencies of 1.0 and 3.3 cycles per second. Measurement of the in-phase and out-of-phase rolling and yawing moments was made in increments of 4° for an angle-of-attack range of 0° to 32°. Inertia effects were eliminated from the data by subtracting wind-off measurements from wind-on measurements. The in-phase and out-of-phase measurements were converted to the derivatives $C_{n_{r,\omega}} - C_{n_{\dot{\beta},\omega}}$, $C_{l_{r,\omega}} - C_{l_{\dot{\beta},\omega}}$, $C_{n_{\beta,\omega}} + k^2 C_{n_{\dot{r},\omega}}$, and $C_{l_{\beta,\omega}} + k^2 C_{l_{\dot{r},\omega}}$. The relatively complicated forms result from the combination β and ψ motion used for these tests.

Corrections

The static tests made utilizing the electromechanical balances were corrected for the effects of tunnel jet boundary and tunnel blockage by the methods of references 9 and 10, respectively. No jet boundary or blockage corrections were applied to the static or oscillatory data measured by the strain gage. Turbulence or strut-interference effects were not taken into account; and although the latter may have been of a sizable magnitude at the higher angles of attack, it is believed that the incremental differences at the higher angles would not be affected by turbulence or strut interference.

RESULTS AND DISCUSSION

Presentation of Results

The results of the investigation are given in figures 5 to 29. Table I gives information as to the content of each figure. The aerodynamic coefficients in figures 5, 6, and 7 are based on static data obtained from the electromechanical balance system. The remainder of the data were obtained from strain-gage tests.

In this paper only the effects of leading-edge radius and profile thickness are treated. Frequency and amplitude effects have been discussed in references 1, 3, 8, 11, and 12.

Effects of Leading-Edge Radius

The basic data (figs. 9 to 16) show that the effects of leading-edge radius on the combination lateral stability derivatives $C_{l_{r,\omega}} - C_{l_{\dot{\beta},\omega}}$ and $C_{n_{r,\omega}} - C_{n_{\dot{\beta},\omega}}$ were small at angles of attack below approximately 12° for the rolling-moment derivative and below approximately 16° for the yawing-moment derivative. At the larger angles of attack, however, an increase in leading-edge radius generally caused decreases in the magnitudes of the derivatives. These differences were not as large as the decreases noted in reference 1. It appears, therefore, that the differences in airfoil sections (65A003 and flat plate) of reference 1, as well as leading-edge radius, have a significant effect on the magnitudes of the oscillatory derivatives.

The decreases in the absolute values of $-\left(C_{n_{r,\omega}} - C_{n_{\dot{\beta},\omega}}\right)$ and $C_{l_{r,\omega}} - C_{l_{\dot{\beta},\omega}}$ with increase in leading-edge radius were largest at the lowest frequencies and highest angles of attack, where frequency-dependent derivatives of large magnitude are usually obtained. There was generally a larger decrease in the damping-in-yaw derivative when the sharp leading edge was given a small radius (compare leading-edge radii of zero and 0.115) than when the leading-edge radius was increased by larger increments from other than zero radius. (See fig. 18.) This trend was erratic for an angle of attack of 32° at $k = 0.033$ and 0.066, and these data are therefore not included in figure 18. The effect of leading-edge radius on the derivatives $C_{n_{\beta,\omega}} + k^2 C_{n_{\dot{r},\omega}}$ and $C_{l_{\beta,\omega}} + k^2 C_{l_{\dot{r},\omega}}$ varied in proportion to angle of attack, the largest effects occurring at the moderate and higher angles of attack. The effect of the increase in leading-edge radius was to decrease these derivatives. The decrease was most pronounced at the higher frequencies throughout the angle-of-attack range. The static derivatives C_{n_β} and C_{l_β} (fig. 17) exhibited the same trends with increase in leading-edge radius as was shown by the oscillatory derivatives. It should also be noted that the oscillation data approached the static data as the frequency was reduced. (See fig. 28.) Theoretical values calculated by the procedures of references 13 and 14 are shown to be in reasonable agreement with experimental values in the low angle-of-attack range.

Effects of Profile Thickness

The effects of profile thickness on the lateral stability derivatives were appreciably larger for the rolling-moment derivatives than for the yawing-moment derivatives and were confined primarily to the higher angles of attack except for the derivative $C_{n_{\beta,\omega}} + k^2C_{n_{\dot{r},\omega}}$, where the effects were more or less proportional to angle of attack (figs. 19 to 26).

The derivative $C_{n_{r,\omega}} - C_{n_{\dot{\beta},\omega}}$ showed essentially no change with variation in profile thickness except at the lowest frequencies ($k = 0.033$ and 0.066) and the highest angles of attack, where maximum damping was obtained for the 5-percent-thick wing. The derivative $C_{l_{r,\omega}} - C_{l_{\dot{\beta},\omega}}$ increased quite appreciably with increase in profile thickness at the higher angles of attack. The increase was greatest at the low frequencies where the derivative had the largest values.

The directional stability derivative $C_{n_{\beta,\omega}} + k^2C_{n_{\dot{r},\omega}}$ showed a definite trend to decrease with increase in profile thickness and the effective dihedral parameter $C_{l_{\beta,\omega}} + k^2C_{l_{\dot{r},\omega}}$ showed large and consistent thickness effects for angles of attack above 8°. An increase in thickness generally decreased the dihedral effect. The static derivatives C_{l_β} and C_{n_β} (fig. 27) exhibited the same trends with increase in thickness as was shown by the corresponding oscillatory derivatives. Theoretical values are also shown.

Frequency Effects

Figures 28 and 29 show typical frequency effects for delta wings with leading-edge radii of 0 and 1.582 percent chord. The high-frequency values approach the derivatives estimated from the procedures of references 13 and 14 which are based on linear-theory concepts, and the low-frequency values approach the measured static values. The two circumstances have been noted by other investigators (for example, ref. 1) and indicate that for the high-frequency range the changes in flow that are normally expected do not have sufficient time to develop, but that there is sufficient time for flow breakdown to occur at the lower frequencies, and the steady-state condition is approached.

Reynolds Number Effects

In an evaluation of the data presented herein, the fact that the results were obtained at a relatively low Reynolds number should be considered. Other investigations have shown that, at least for static derivatives, increasing Reynolds number extends the linear range of the aerodynamic parameters plotted against angle of attack. (See ref. 15, for example.) These effects have been found to be more pronounced for airfoils with large leading-edge radii than for airfoils with small leading-edge radii. Therefore, the same trends would appear likely to apply to the present investigation, and the results for the larger leading-edge radii would probably be most affected.

CONCLUSIONS

The results of tests to determine the effects of variation in leading-edge radius and profile thickness on the lateral stability derivatives of a 60° delta wing indicate the following conclusions:

1. Noticeable decreases occurred in all the derivatives as a result of increases in leading-edge radius at angles of attack above approximately 12°.

2. An increase in profile thickness caused appreciable increases in $C_{l_{r,\omega}} - C_{l_{\dot{\beta},\omega}}$ and large decreases in effective dihedral, $\left(C_{l_{\beta,\omega}} + k^2 C_{l_{\dot{r},\omega}}\right)$, at angles of attack above 8°.

3. Profile-thickness effects were small for the yawing-moment derivatives.

4. The static derivatives C_{l_β} and C_{n_β}, showed essentially the same effects of leading-edge radius and profile thickness as the oscillatory derivatives.

Langley Aeronautical Laboratory,
National Advisory Committee for Aeronautics,
Langley Field, Va., March 14, 1958.

REFERENCES

1. Lichtenstein, Jacob H., and Williams, James L.: Effects of Frequency of Sideslipping Motion on the Lateral Stability Derivatives of a Typical Delta Wing Airplane. NACA RM L57F07, 1957.

2. Furlong, G. Chester, and McHugh, James G.: A Summary and Analysis of the Low-Speed Longitudinal Characteristics of Swept Wings at High Reynolds Number. NACA Rep. 1339, 1957. (Supersedes NACA RM L52D16.)

3. Campbell, John P., Johnson, Joseph L., Jr., and Hewes, Donald E.: Low-Speed Study of the Effect of Frequency on the Stability Derivatives of Wings Oscillating in Yaw With Particular Reference to High Angle-of-Attack Conditions. NACA RM L55H05, 1955.

4. Örnberg, Torsten: A Note on the Flow Around Delta Wings. KTH-Aero TN 38, Roy. Inst. of Tech., Div. of Aero., Stockholm, Sweden, 1954.

5. Pocock, P. J., and Laundry, W. E.: Some Aerodynamic Characteristics of Delta Wings at Low Speeds. Second Canadian Symposium on Aerodynamics. Inst. of Aerophysics, Univ. of Toronto. Feb. 25-26, 1954, pp. 39-68.

6. Foster, Gerald V.: Effects of Leading-Edge Radius on the Longitudinal Stability of Two 45° Sweptback Wings Incorporating Leading-Edge Camber as Influenced by Reynolds Numbers up to 8.00×10^6 and Mach Numbers up to 0.290. NACA RM L55H04, 1955.

7. Foster, Gerald V., and Schneider, William C.: Effects of Leading-Edge Radius on the Longitudinal Stability of Two 45° Sweptback Wings as Influenced by Reynolds Numbers up to 8.20×10^6 and Mach Numbers up to 0.303. NACA RM L55F06, 1955.

8. Queijo, M. J., Fletcher, Herman S., Marple, C. G., and Hughes, F. M.: Preliminary Measurements of the Aerodynamic Yawing Derivatives of a Triangular, a Swept, and an Unswept Wing Performing Pure Yawing Oscillations, With a Description of the Instrumentation Employed. NACA RM L55L14, 1956.

9. Silverstein, Abe, and White, James A.: Wind-Tunnel Interference With Particular Reference to Off-Center Positions of the Wing and to the Downwash at the Tail. NACA Rep. 547, 1936.

10. Herriot, John G.: Blockage Corrections for Three-Dimensional-Flow Closed-Throat Wind Tunnels, With Consideration of the Effect of Compressibility. NACA Rep. 995, 1950. (Supersedes NACA RM A7B28.)

11. Fisher, Lewis R.: Experimental Determination of the Effects of Frequency and Amplitude on the Lateral Stability Derivatives for a Delta, a Swept, and an Unswept Wing Oscillating in Yaw. NACA RM L56A19, 1956.

12. Letko, William: Experimental Determination at Subsonic Speeds of the Oscillatory and Static Lateral Stability Derivatives of a Series of Delta Wings With Leading-Edge Sweep From 30° to 86.5°. NACA RM L57A30, 1957.

13. Queijo, M. J.: Theoretical Span Load Distributions and Rolling Moments for Sideslipping Wings of Arbitrary Plan Form in Incompressible Flow. NACA Rep. 1269, 1956. (Supersedes NACA TN 3605.)

14. Toll, Thomas A., and Queijo, M. J.: Approximate Relations and Charts for Low-Speed Stability Derivatives of Swept Wings. NACA TN 1581, 1948.

15. Neely, Robert H., and Conner, D. William: Aerodynamic Characteristics of a 42° Sweptback Wing With Aspect Ratio 4 and NACA 64_1-112 Airfoil Sections at Reynolds Numbers From 1,700,000 to 9,500,000. NACA RM L7D14, 1947.

TABLE I.- INDEX OF FIGURES

Figure	Variables	α, deg	β, deg	t, percent c	L. E. radius, percent c	Yaw amplitude, ψ_o, deg	k
5, 6, 7	C_L, C_D, C_m	Range	0	3, 5, 8	0, 0.115, 0.791, 1.582	---	0
8	C_l, C_n	12, 20, 24, 28, 32	Range	3, 5, 8	0, 0.115, 0.791, 1.582	---	0
9, 10	Oscillatory derivatives	Range	------	3	0, 0.115, 0.791, 1.582	±2	0.066, 0.218
11, 12, 13, 14, 18	Oscillatory derivatives	Range	------	3	0, 0.115, 0.791, 1.582	±6	0.033, 0.066, 0.132, 0.218
15, 16	Oscillatory derivatives	Range	------	3	0, 0.115, 0.791, 1.582	±10	0.066, 0.218
19, 20	Oscillatory derivatives	Range	------	3, 5, 8	0.791	±2	0.066, 0.218
21, 22, 23, 24	Oscillatory derivatives	Range	------	3, 5, 8	0.791	±6	0.033, 0.066, 0.132, 0.218
25, 26	Oscillatory derivatives	Range	------	3, 5, 8	0.791	±10	0.066, 0.218
17	Comparison of theoretical and static values of C_{n_β} and C_{l_β}	Range	±2, ±6	3	0, 0.115, 0.791, 1.582	---	0
27	Comparison of theoretical and static values of C_{n_β} and C_{l_β}	Range	±2, ±6	3, 5, 8	0.791	---	0
28	Comparison of theoretical, static and oscillatory derivatives	Range	------	3	0	±6	0, 0.033, 0.066, 0.132, 0.218
29	Comparison of theoretical, static and oscillatory derivatives	Range	------	3	1.582	±6	0, 0.033, 0.066, 0.132, 0.218

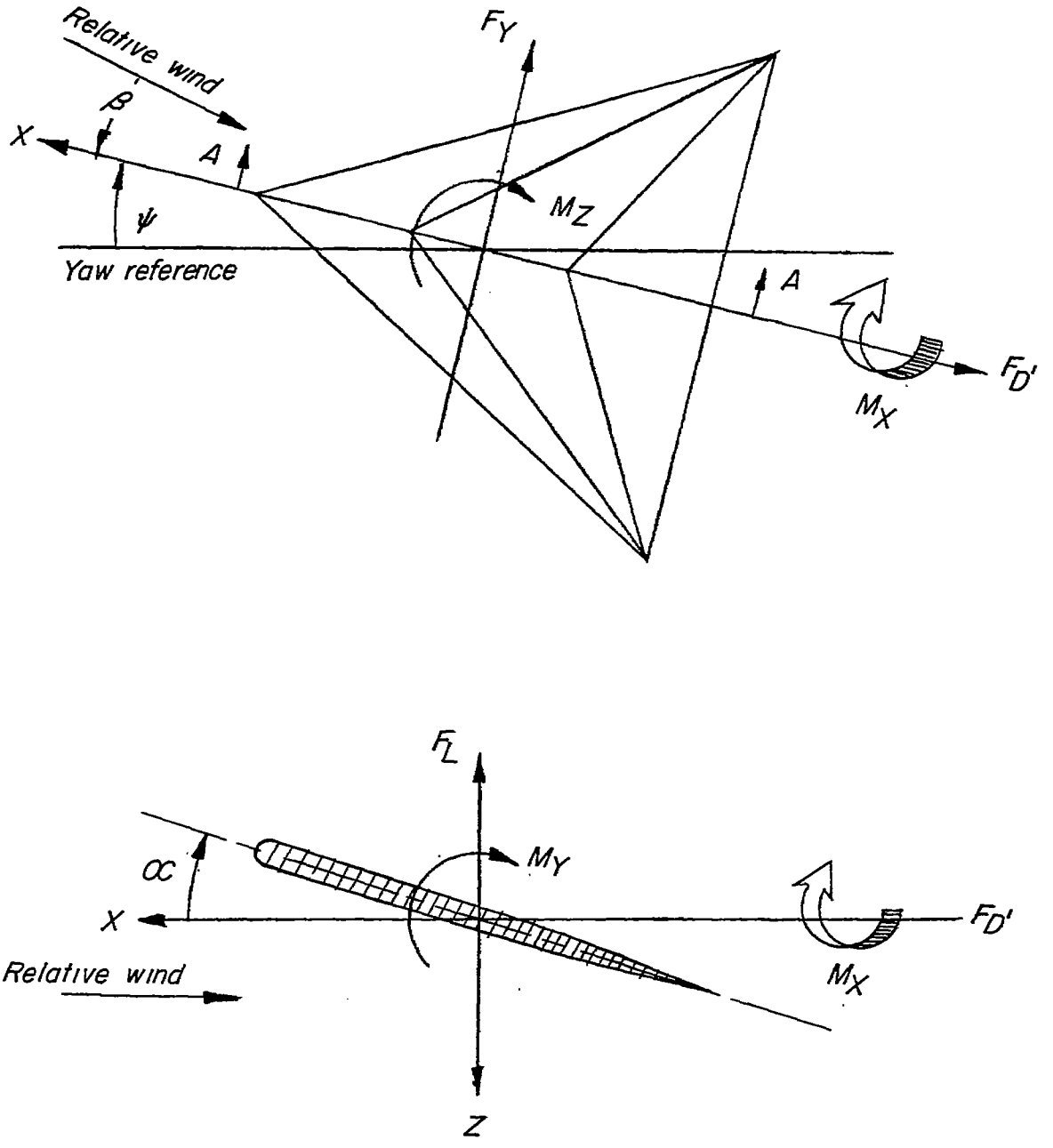

Figure 1.- System of stability axes. Arrows indicate positive sense of forces, moments, and angular displacements.

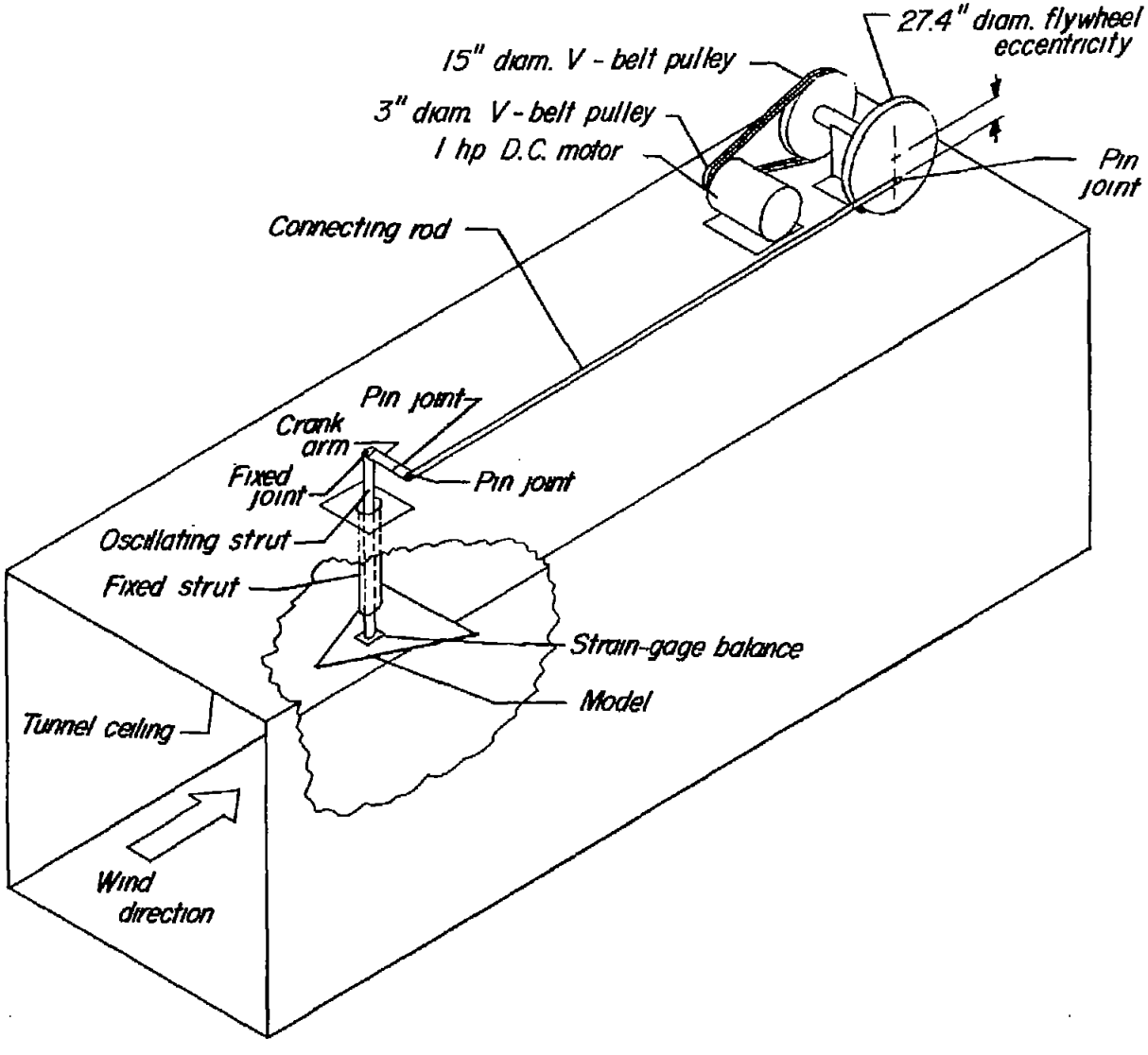

Figure 2.- Sketch of oscillation-in-yaw equipment.

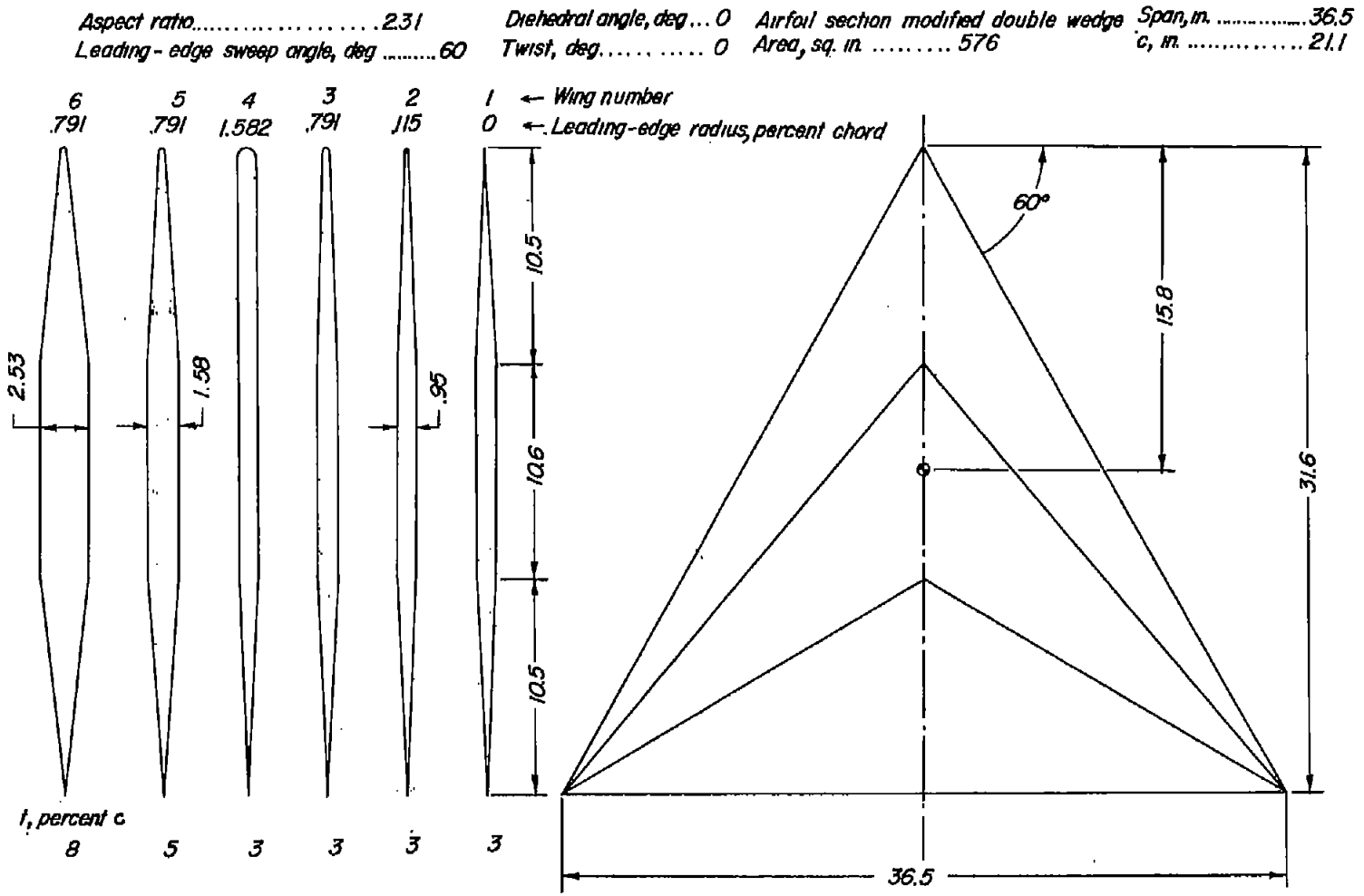

Figure 3.- Sketch of models used in tests. All dimensions are in inches.

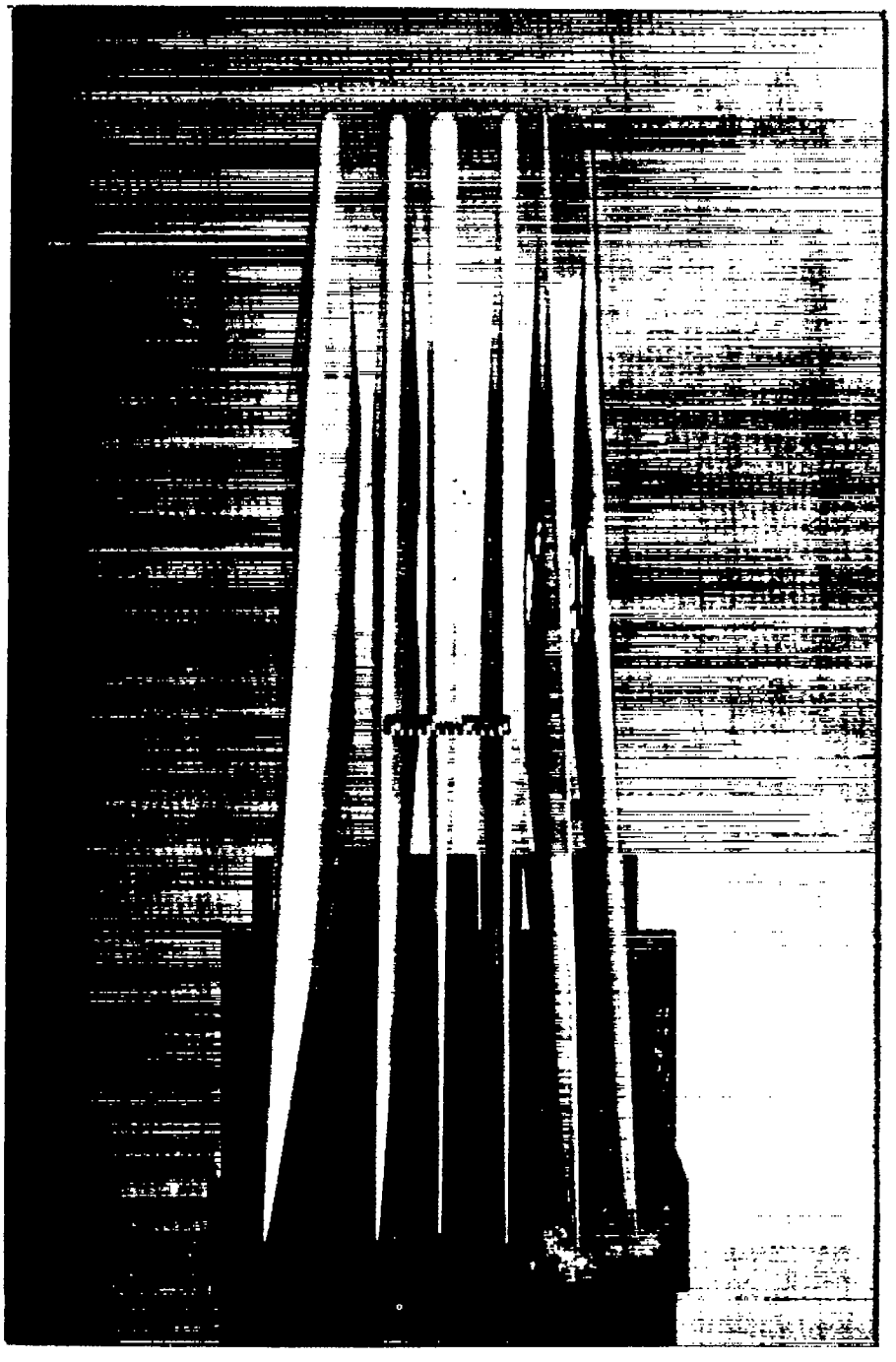

(a) Front view. L-57-955

Figure 4.- Photographs of models.

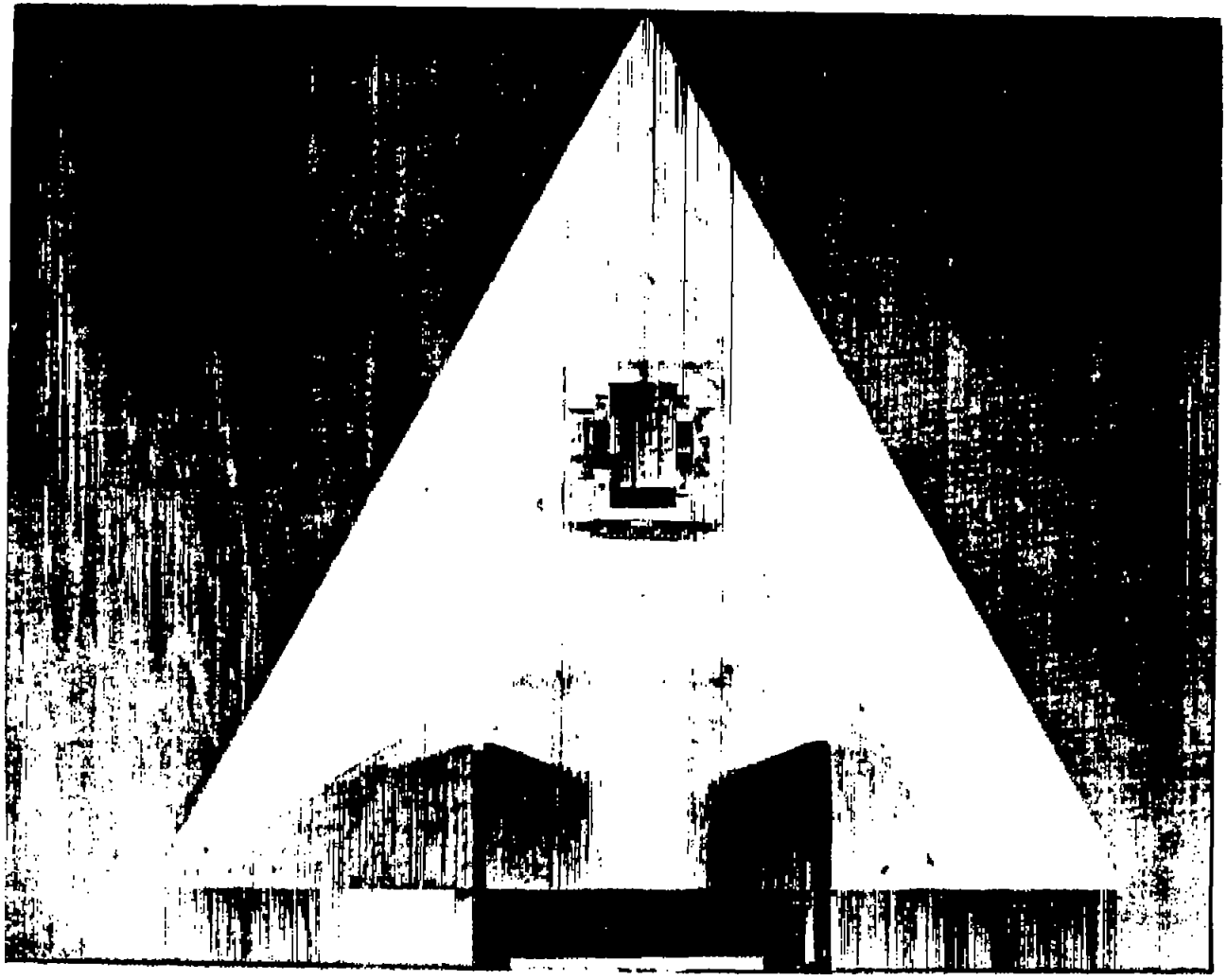

(b) Plan view. L-57-954

Figure 4.- Concluded.

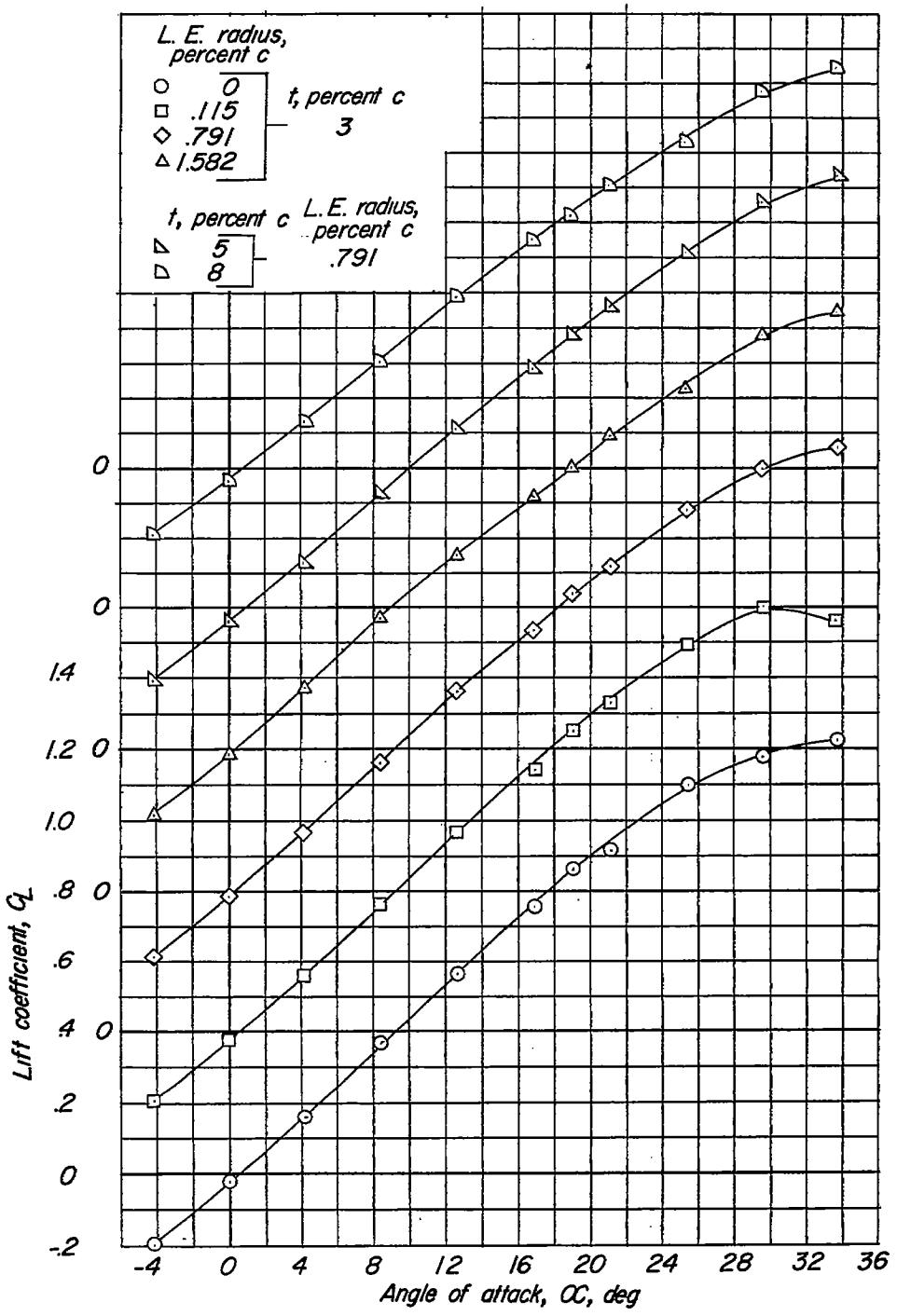

Figure 5.- Lift coefficient as a function of angle of attack for the six 60° delta wings.

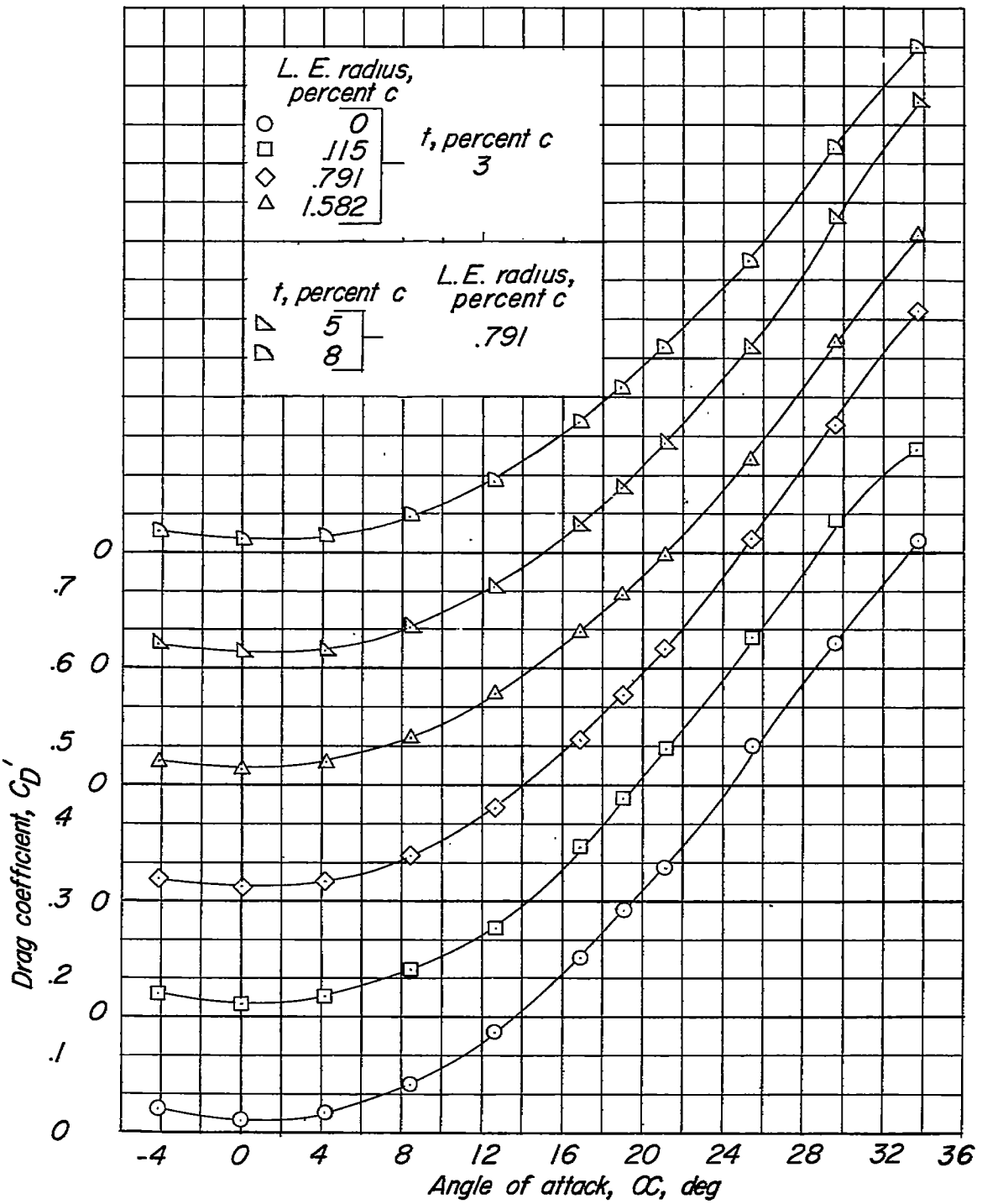

Figure 6.- Drag coefficient as a function of angle of attack for the six 60° delta wings.

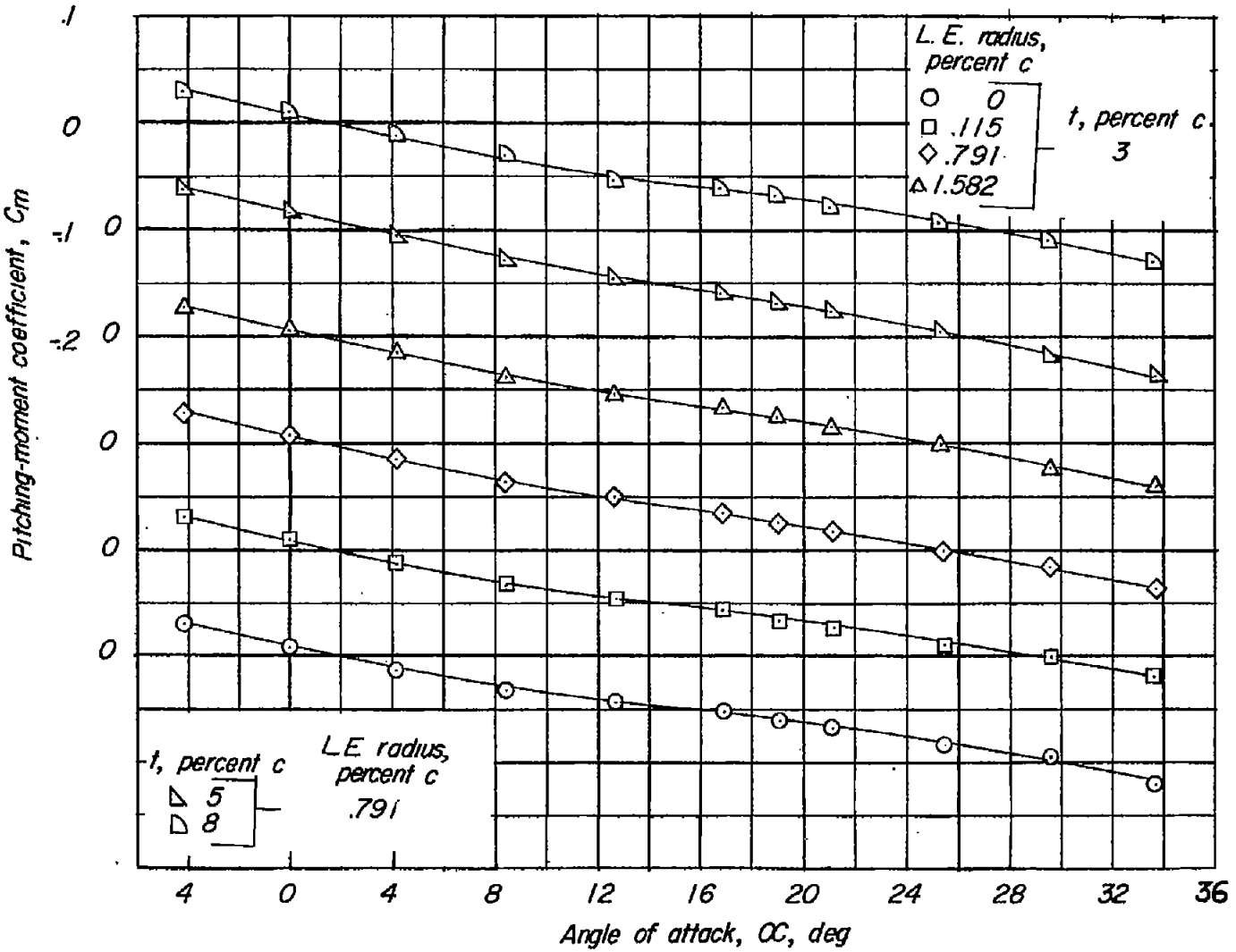

Figure 7.- Pitching-moment coefficient as a function of angle of attack for the six 60° delta wings.

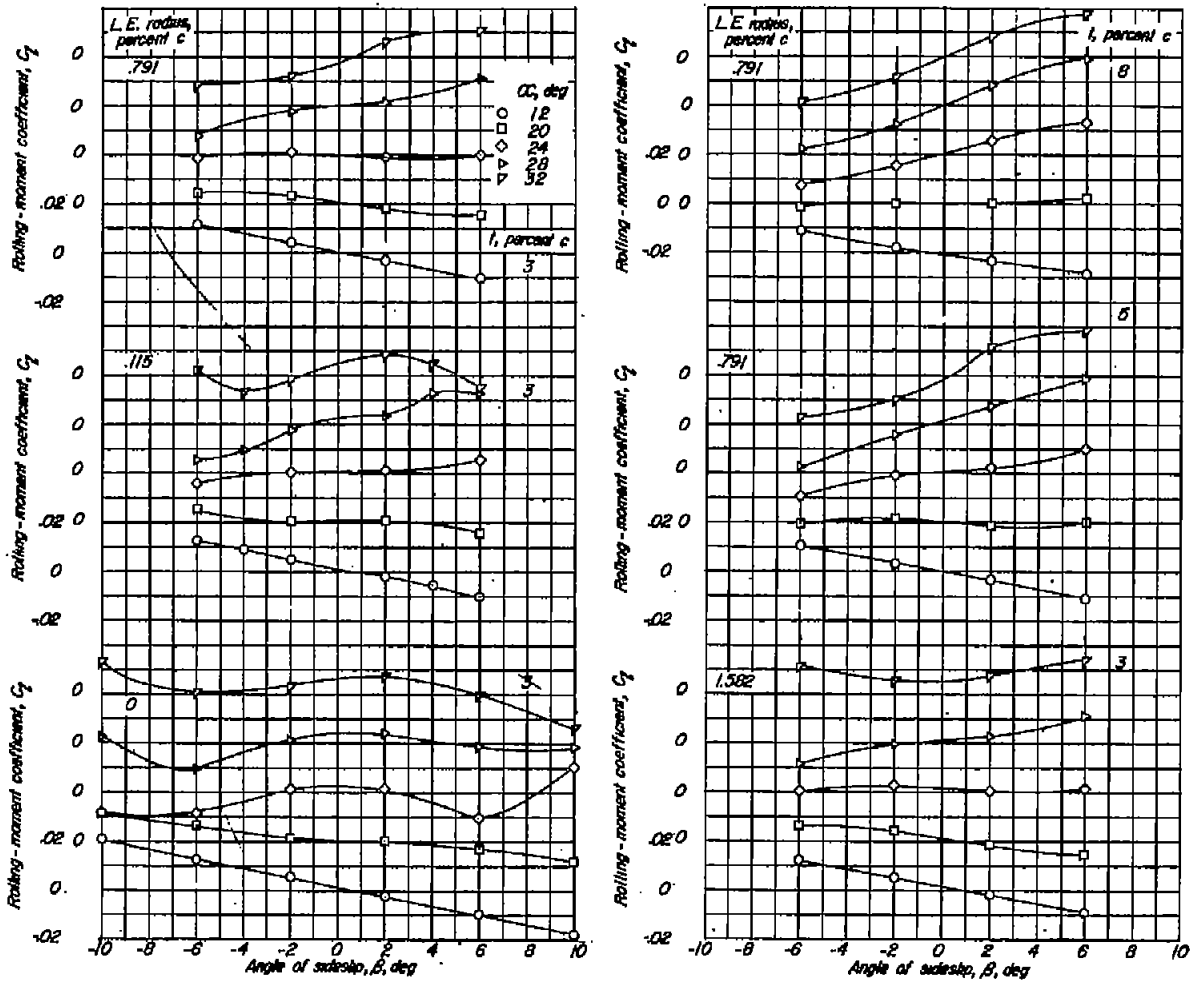

(a) Rolling-moment coefficients.

Figure 8.- Variation of yawing-moment and rolling-moment coefficients with angle of sideslip for the six 60° delta wings.

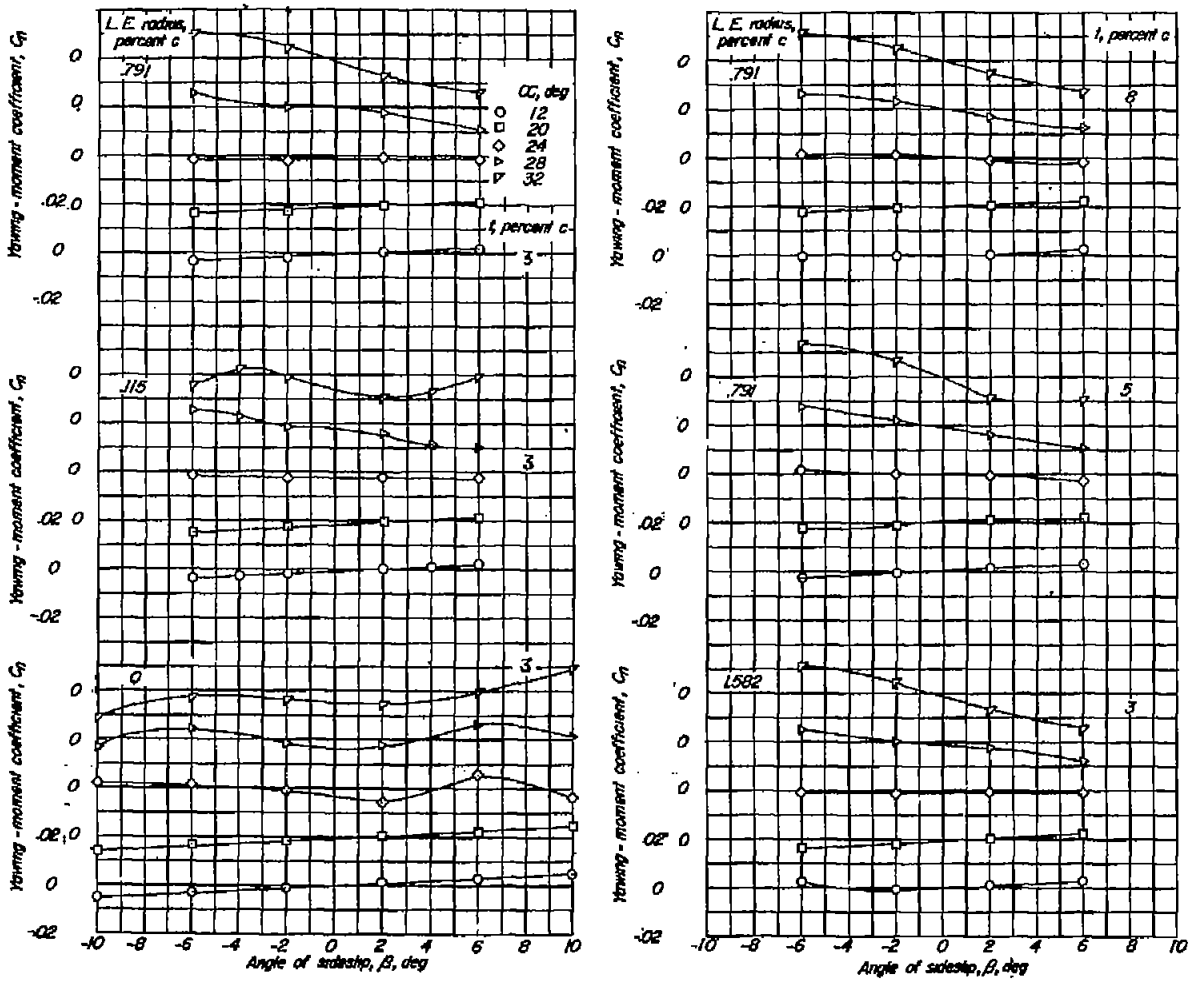

(b) Yawing-moment coefficients.

Figure 8.- Concluded.

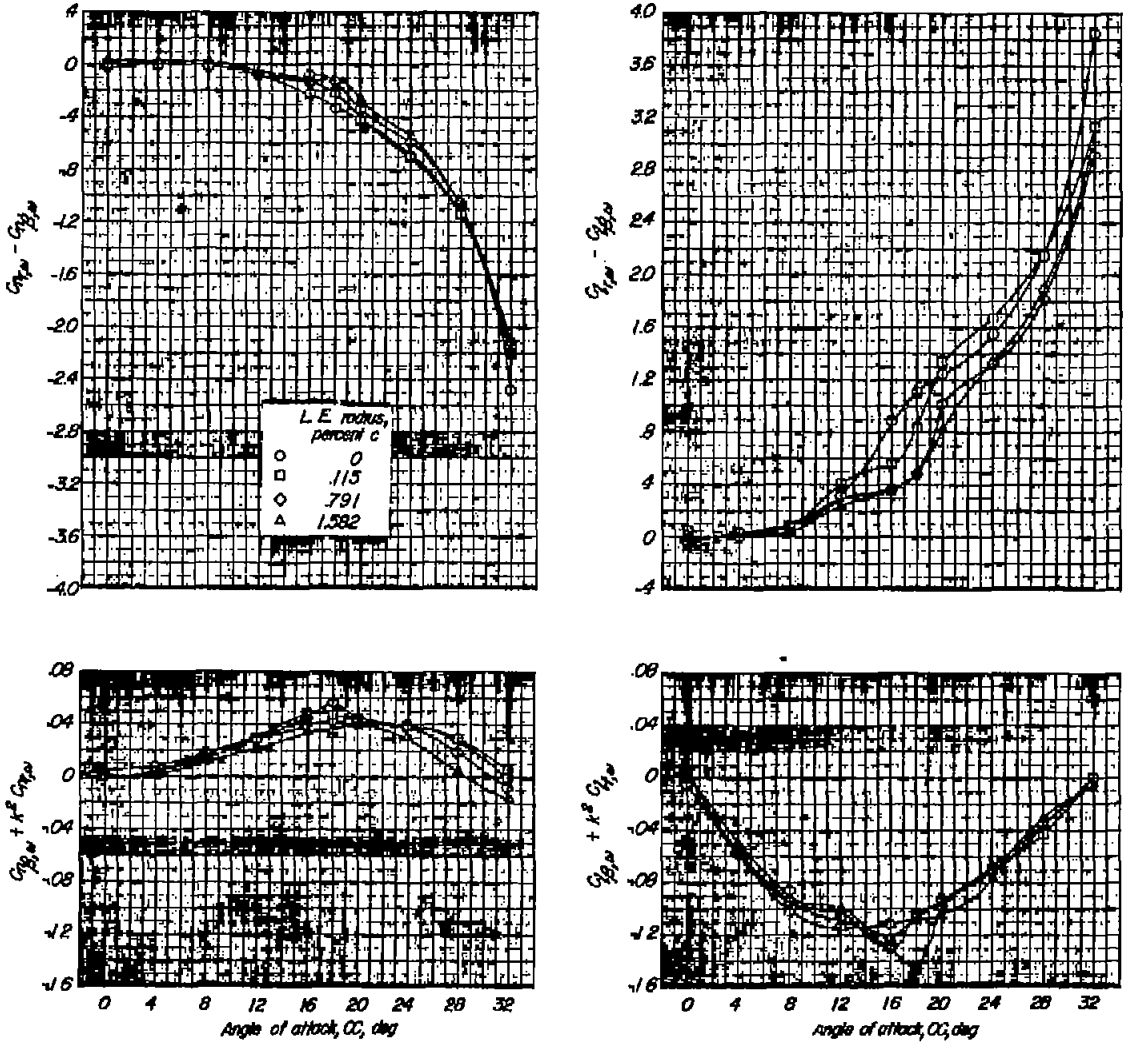

Figure 9.- Effect of leading-edge radius on the oscillatory stability derivatives for a 3-percent-thick 60° delta wing. $\psi_o = \pm 2^\circ$; $k = 0.066$.

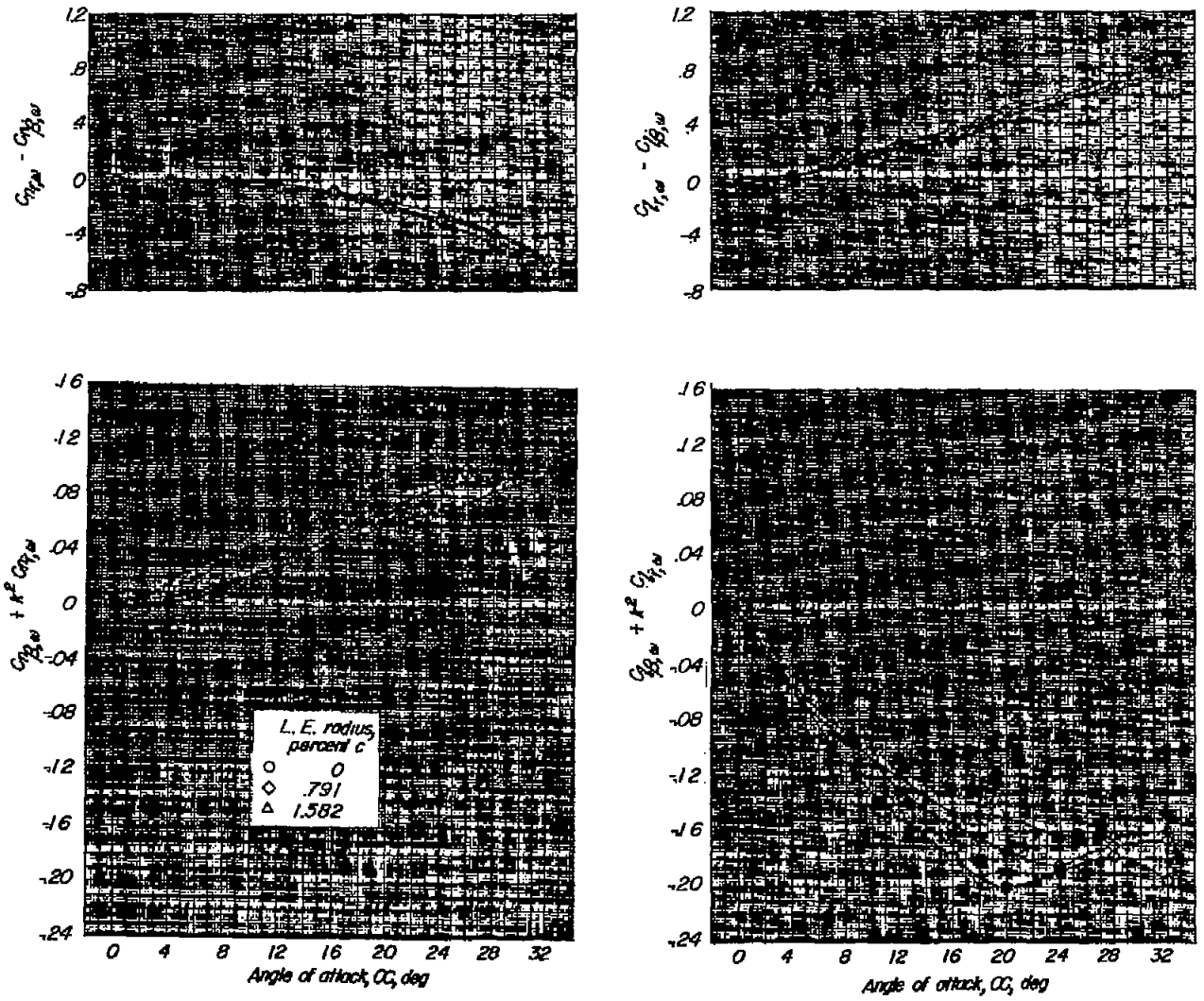

Figure 10.- Effect of leading-edge radius on the oscillatory stability derivatives for a 3-percent-thick 60° delta wing. $\psi_o = \pm 2^\circ$; $k = 0.218$.

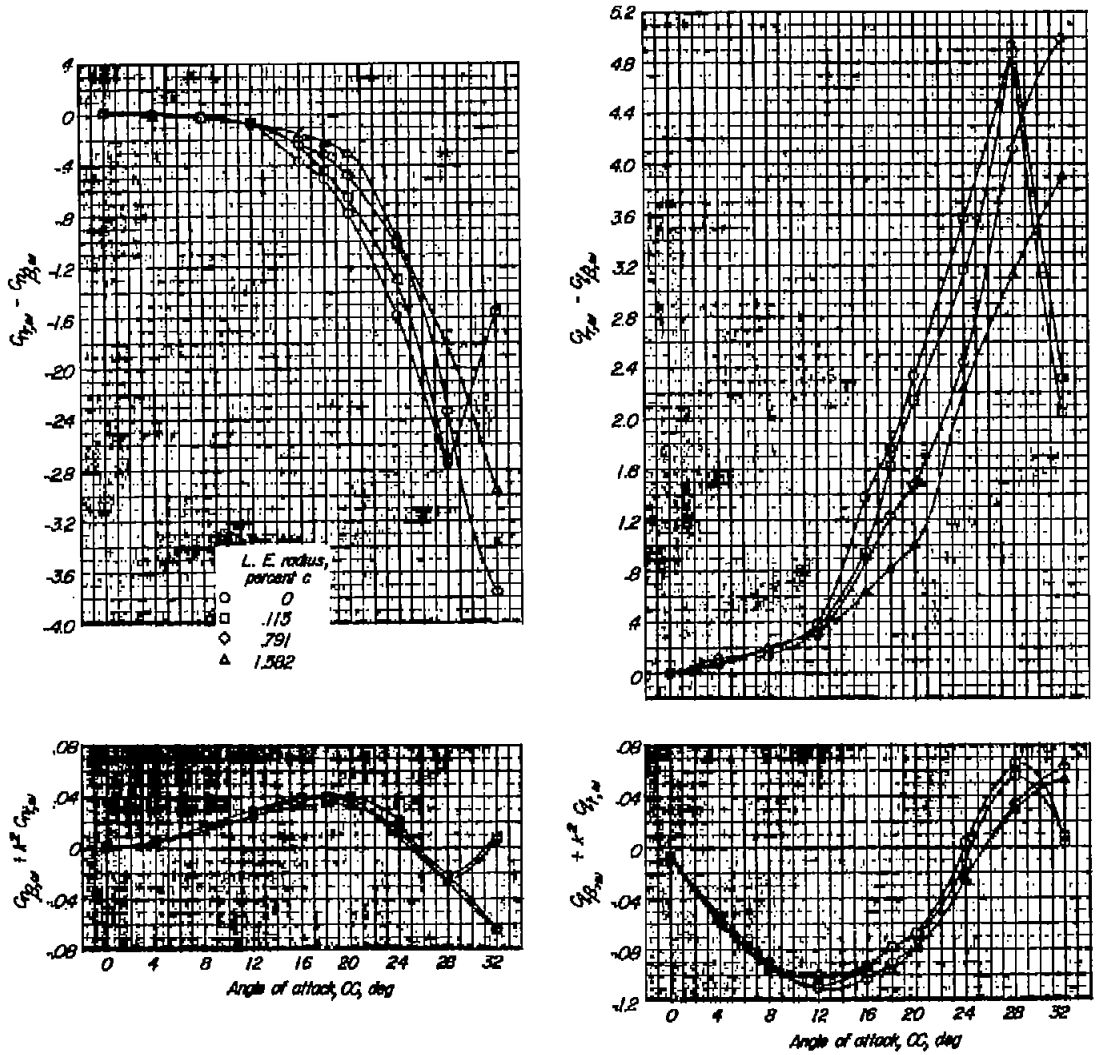

Figure 11.- Effect of leading-edge radius on the oscillatory stability derivatives for a 3-percent-thick 60° delta wing. $\Psi_0 = \pm 6°$; k = 0.033.

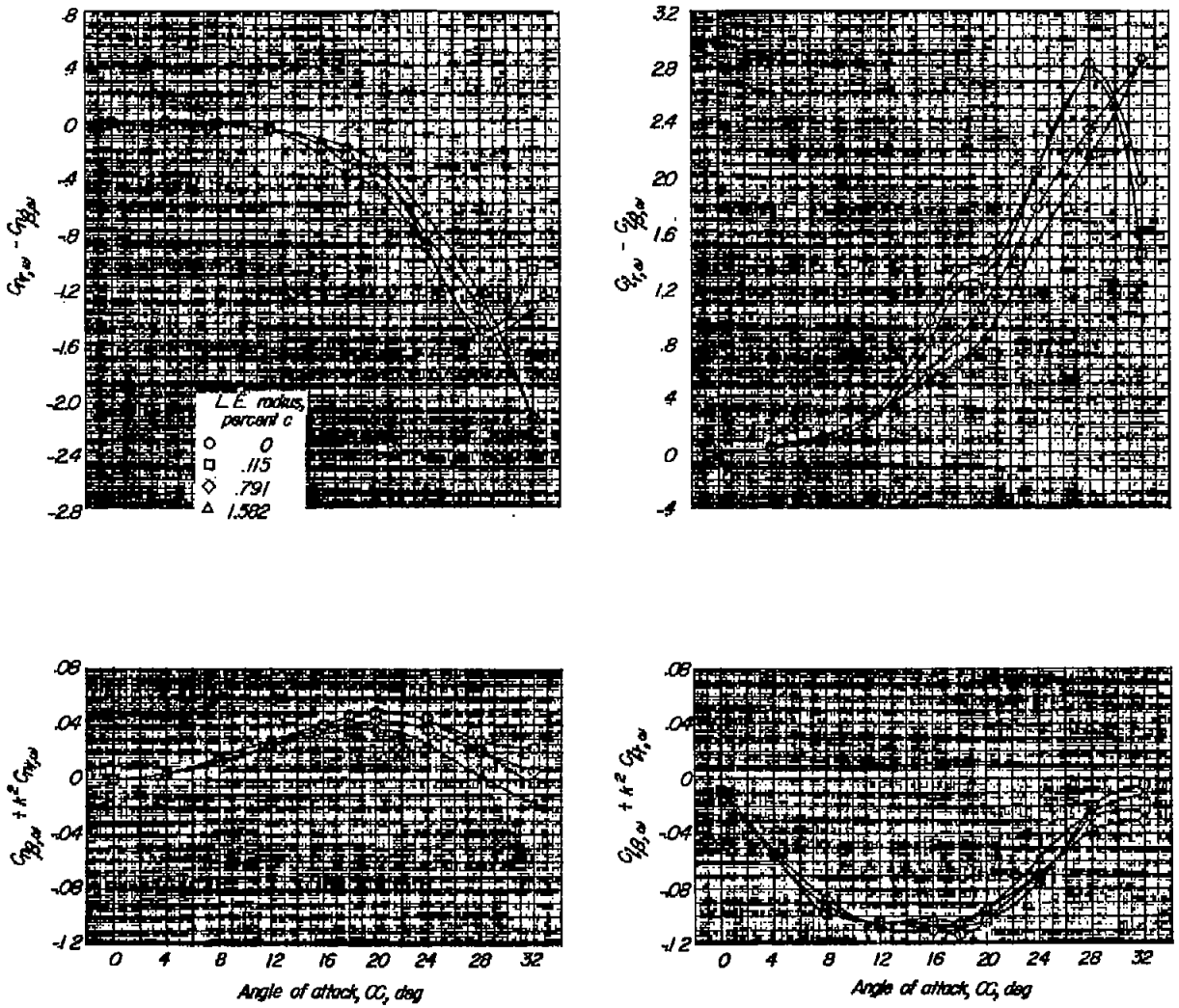

Figure 12.- Effect of leading-edge radius on the oscillatory stability derivatives for a 3-percent-thick 60° delta wing. $\psi_o = \pm 6°$; $k = 0.066$.

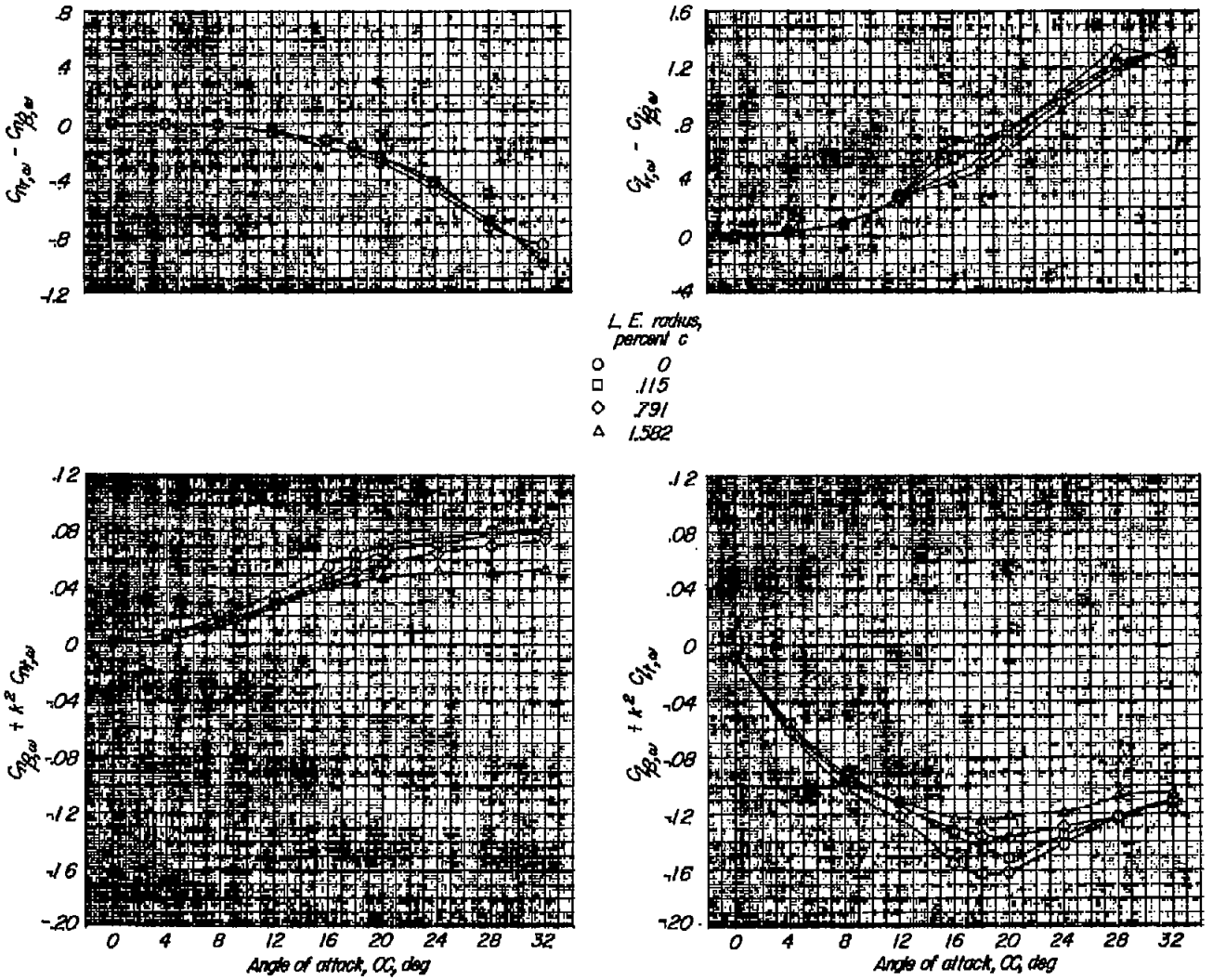

Figure 13.- Effect of leading-edge radius on the oscillatory stability derivatives for a 3-percent-thick 60° delta wing. $\Psi_o = \pm 6°$; k = 0.132.

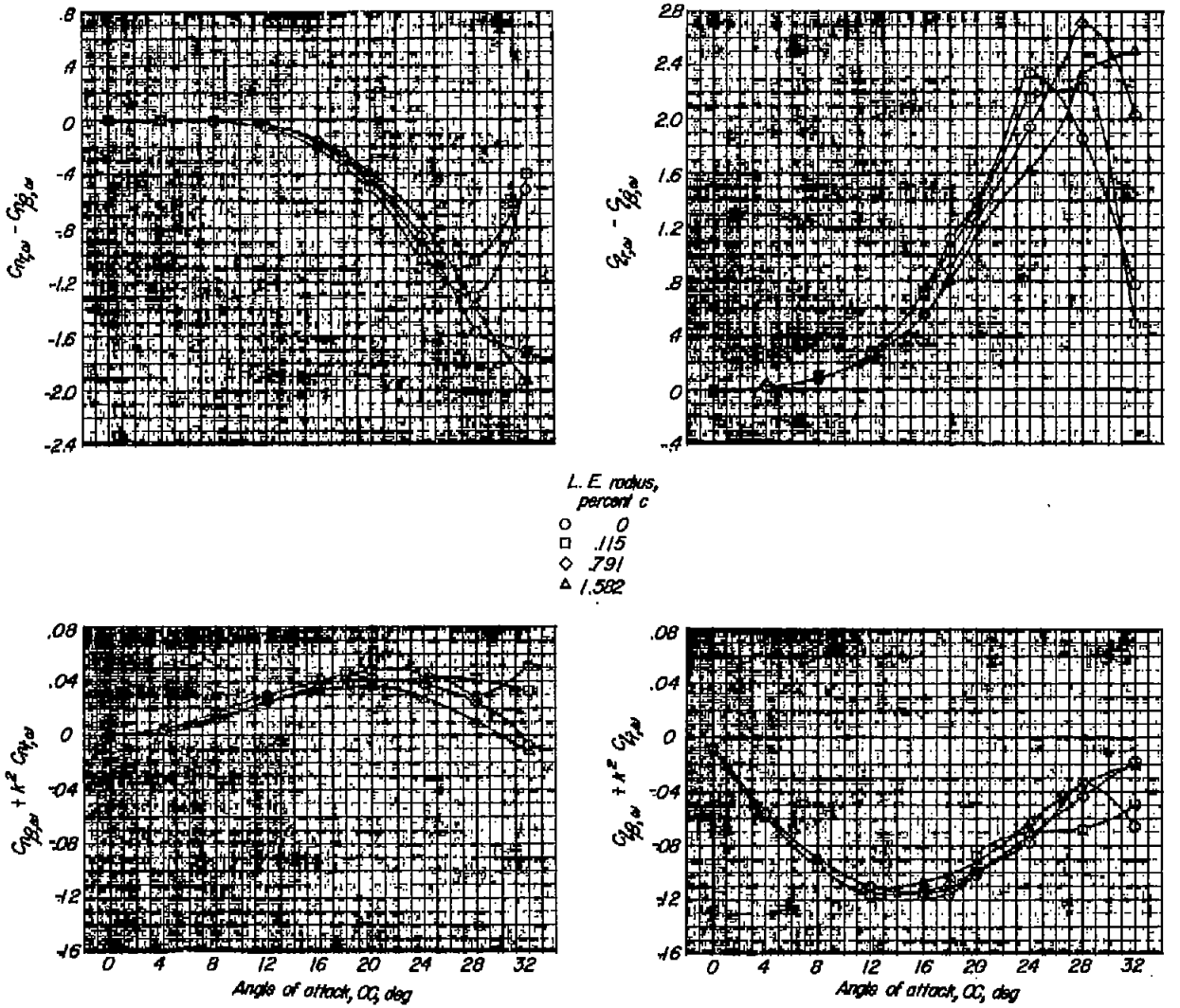

Figure 15.- Effect of leading-edge radius on the oscillatory stability derivatives for a 3-percent-thick 60° delta wing. $\Psi_0 = \pm 10°$; k = 0.066.

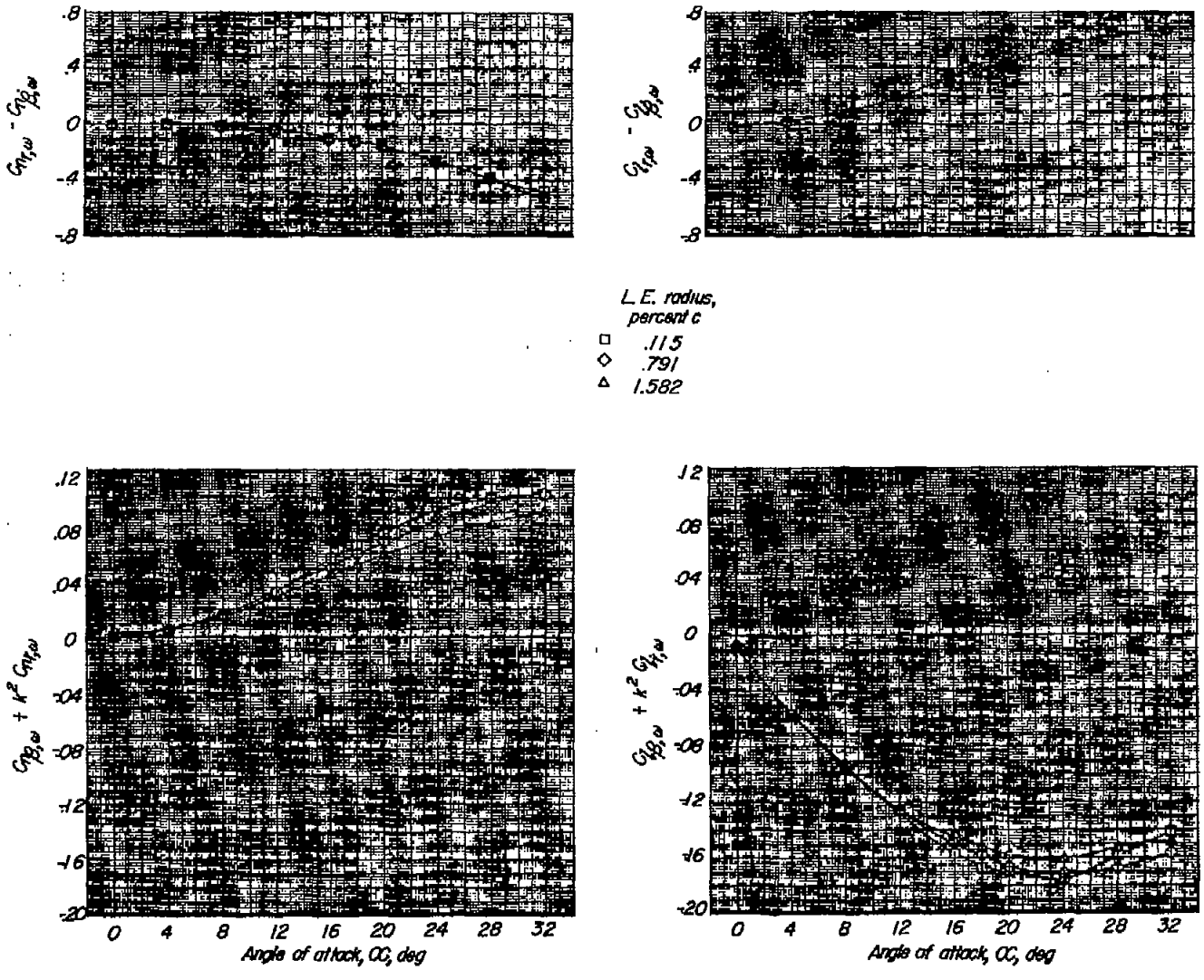

Figure 16.- Effect of leading-edge radius on the oscillatory stability derivatives for a 3-percent-thick 60° delta wing. $\psi_o = \pm 10°$; k = 0.218.

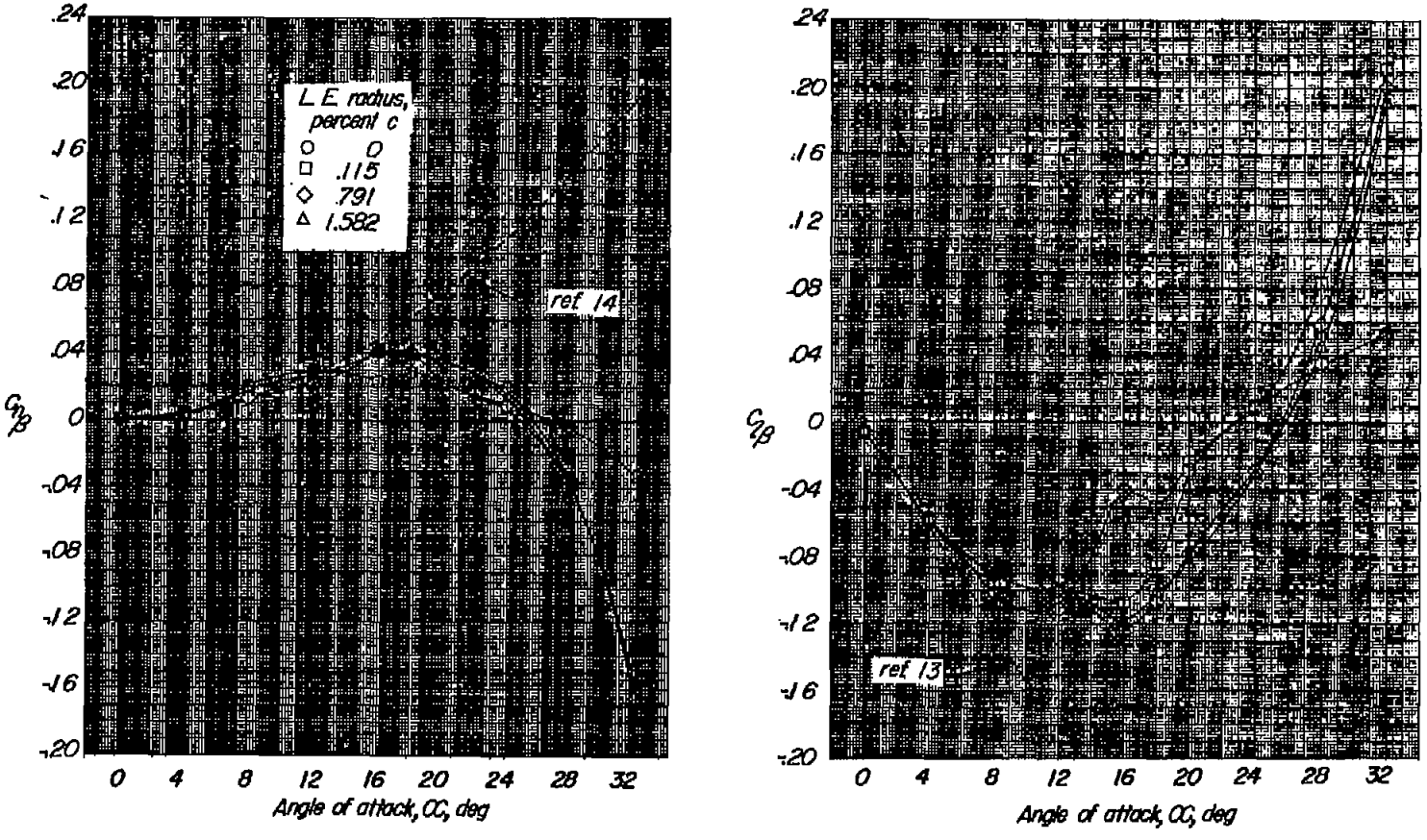

(a) $\Psi_o = \pm 2^\circ$.

Figure 17.- Effect of leading-edge radius on the static stability derivatives for a 3-percent-thick 60° delta wing.

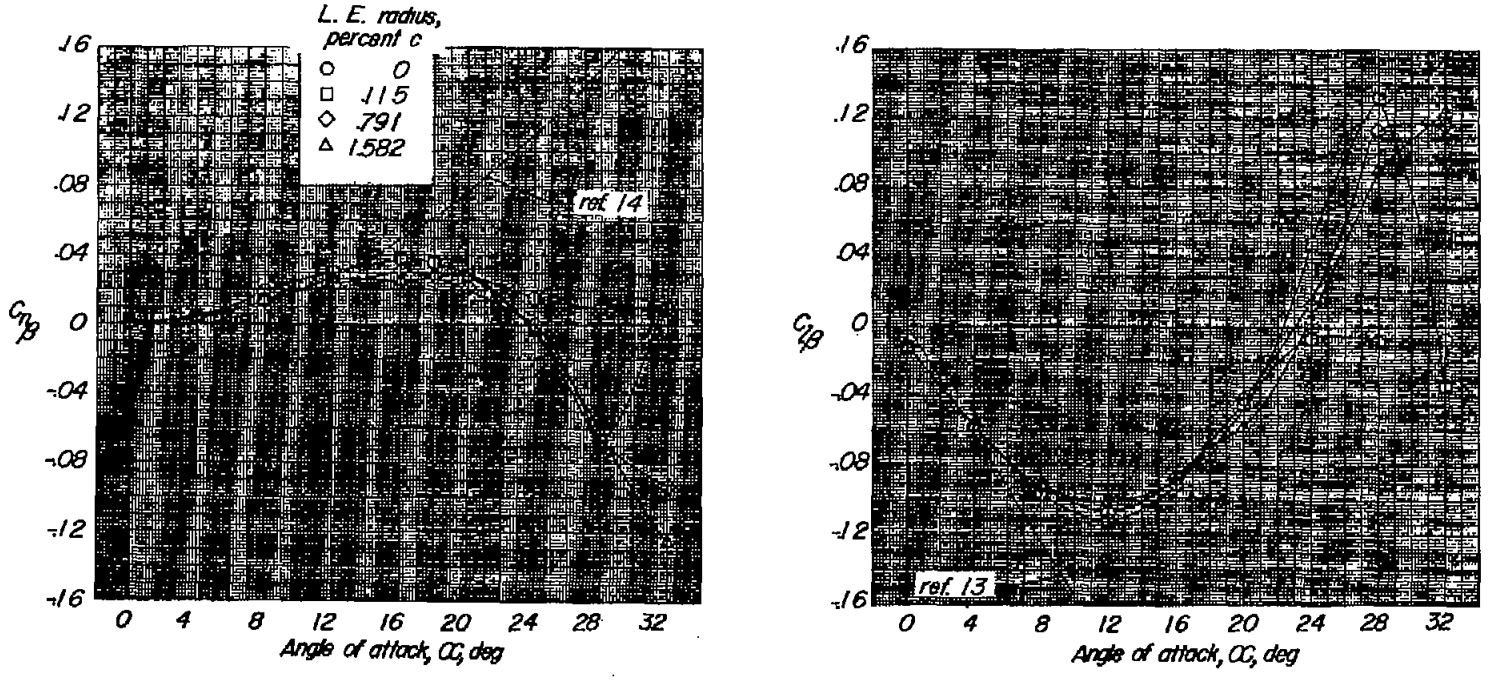

(b) $\Psi_o = \pm 6^\circ$.

Figure 17.- Concluded.

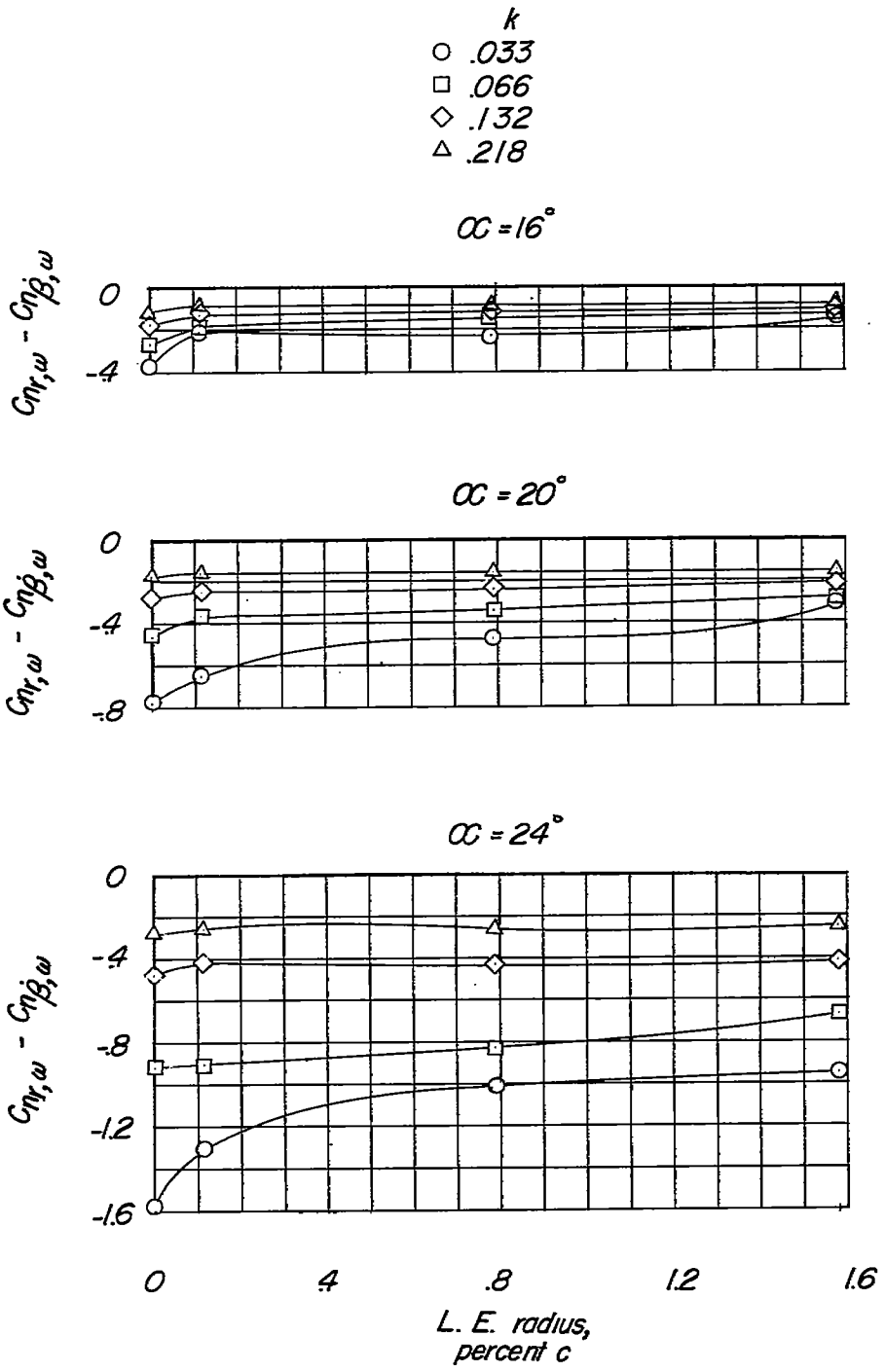

Figure 18.- Effect of leading-edge radius on the damping in yaw for a 3-percent-thick 60° delta wing. $\psi_o = \pm 6°$.

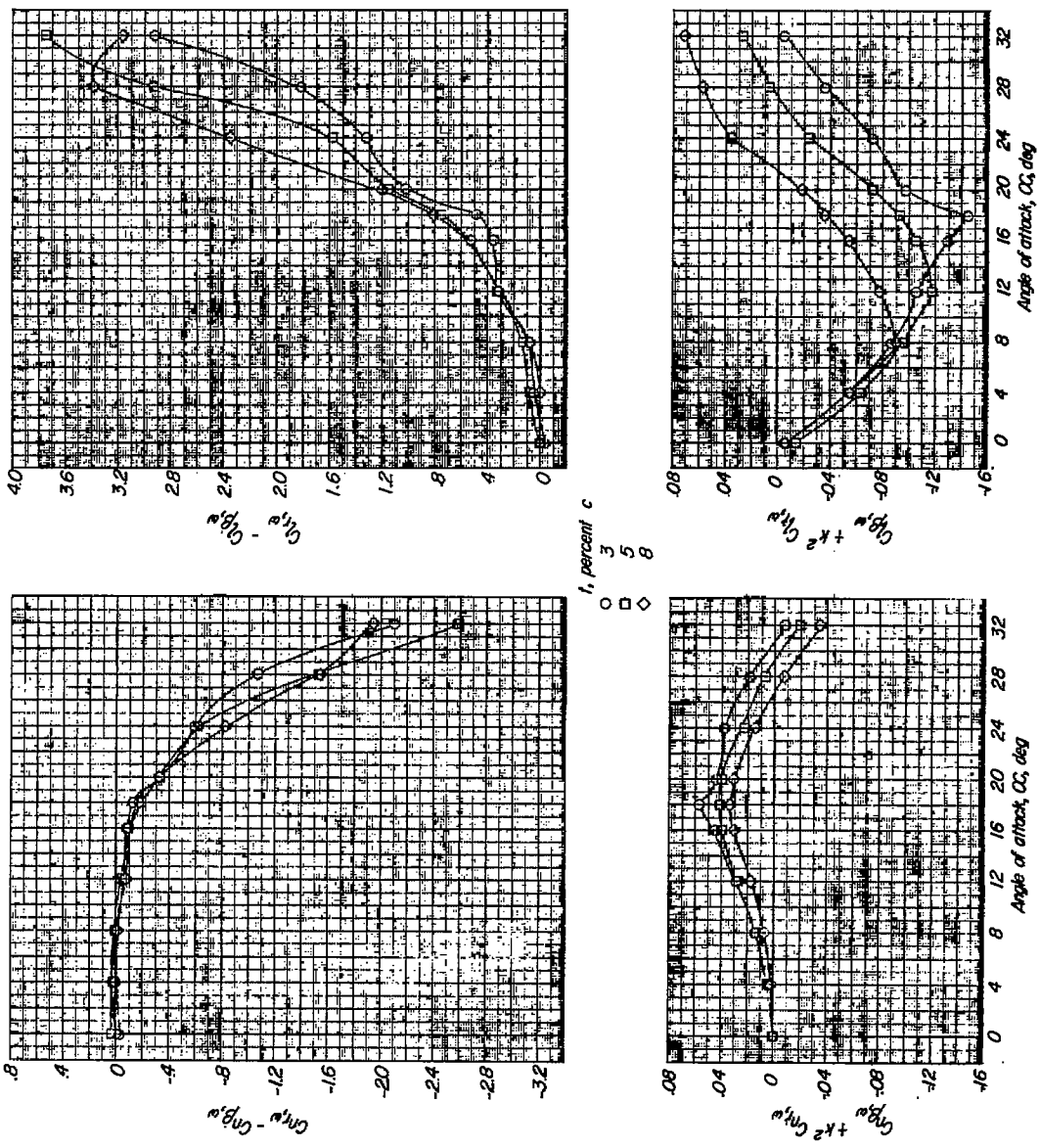

Figure 19.- Effect of profile thickness on the oscillatory stability derivatives for a 60° delta wing with a leading-edge radius of 0.791 percent c. $\psi_o = \pm 2°$; k = 0.066.

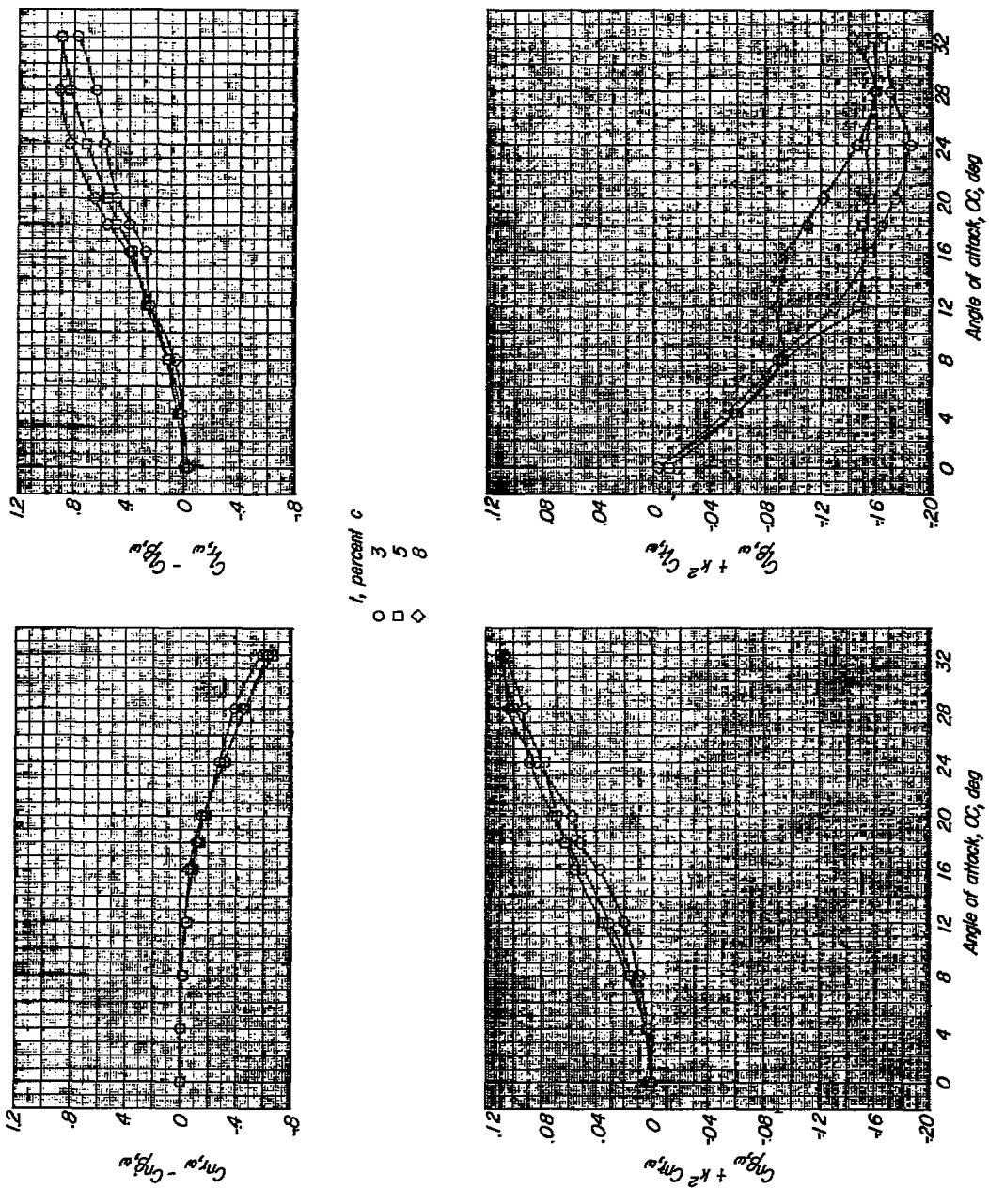

Figure 20.- Effect of profile thickness on the oscillatory stability derivatives for a 60° delta wing with a leading-edge radius of 0.791 percent c. $\psi_o = \pm 2°$; k = 0.218.

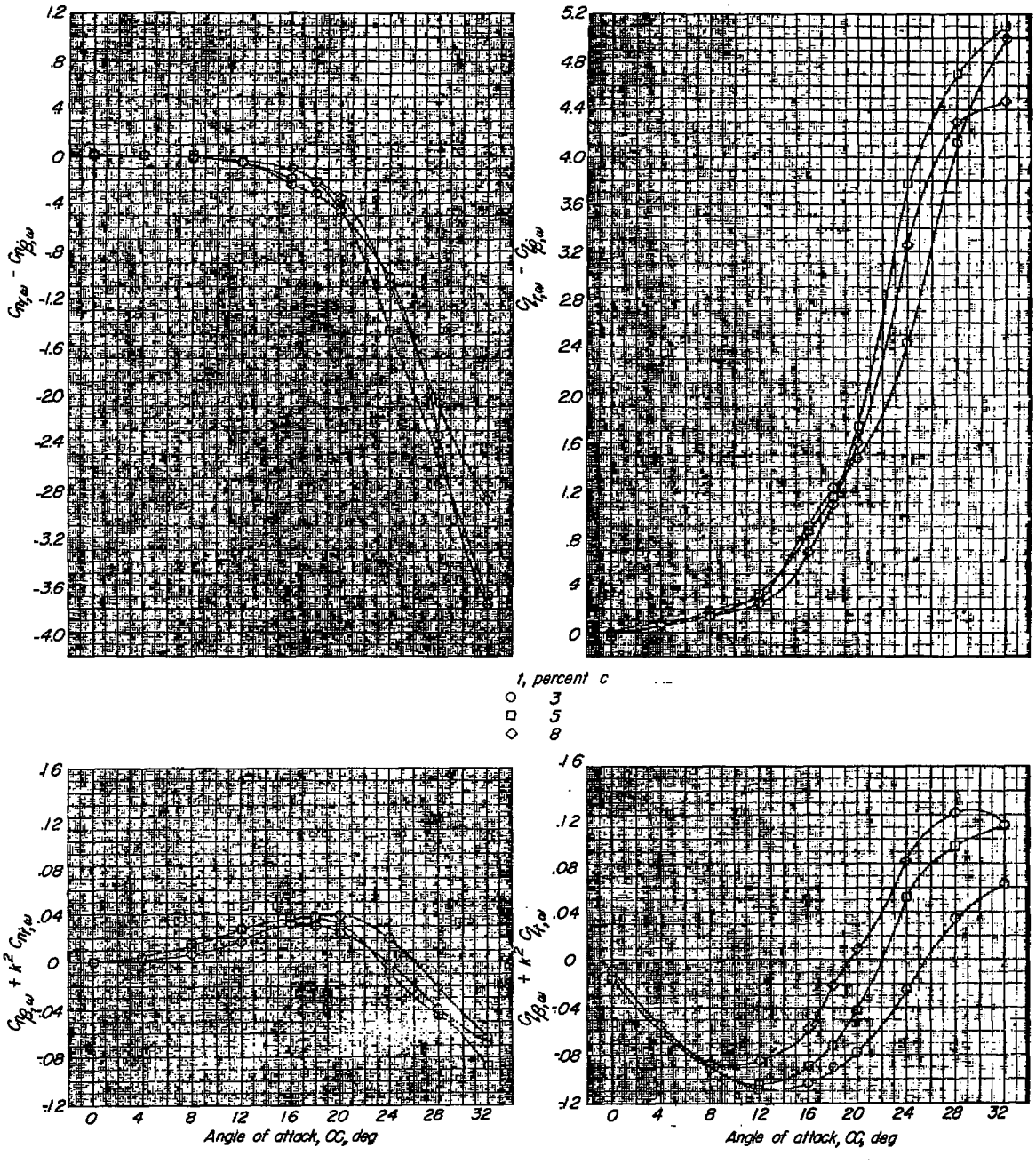

Figure 21.- Effect of profile thickness on the oscillatory stability derivatives for a 60° delta wing with a leading-edge radius of 0.791 percent c. $\psi_o = \pm 6^\circ$; k = 0.033.

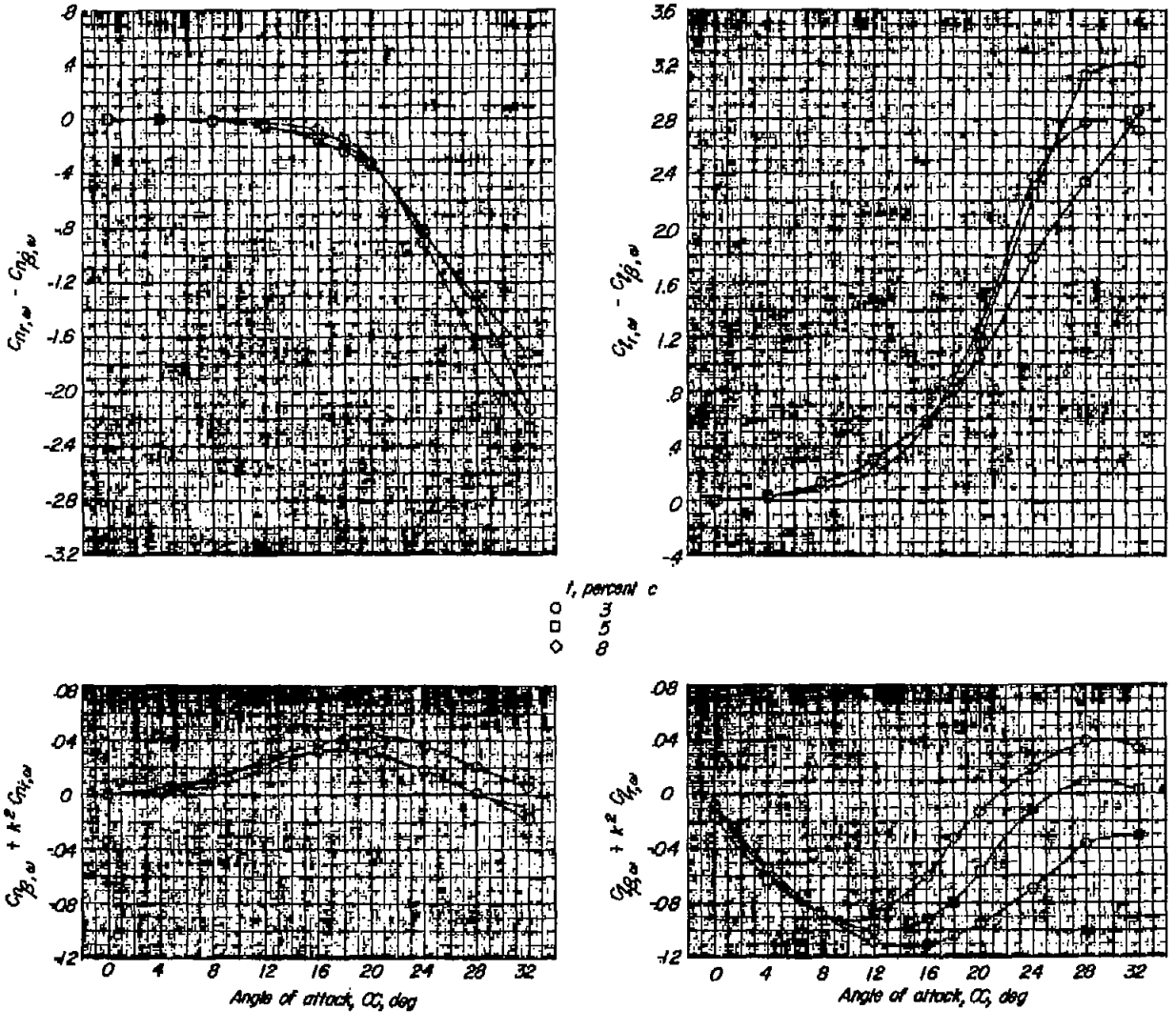

Figure 22.- Effect of profile thickness on the oscillatory stability derivatives for a 60° delta wing with a leading-edge radius of 0.791 percent c. $\psi_o = \pm 6°$; $k = 0.066$.

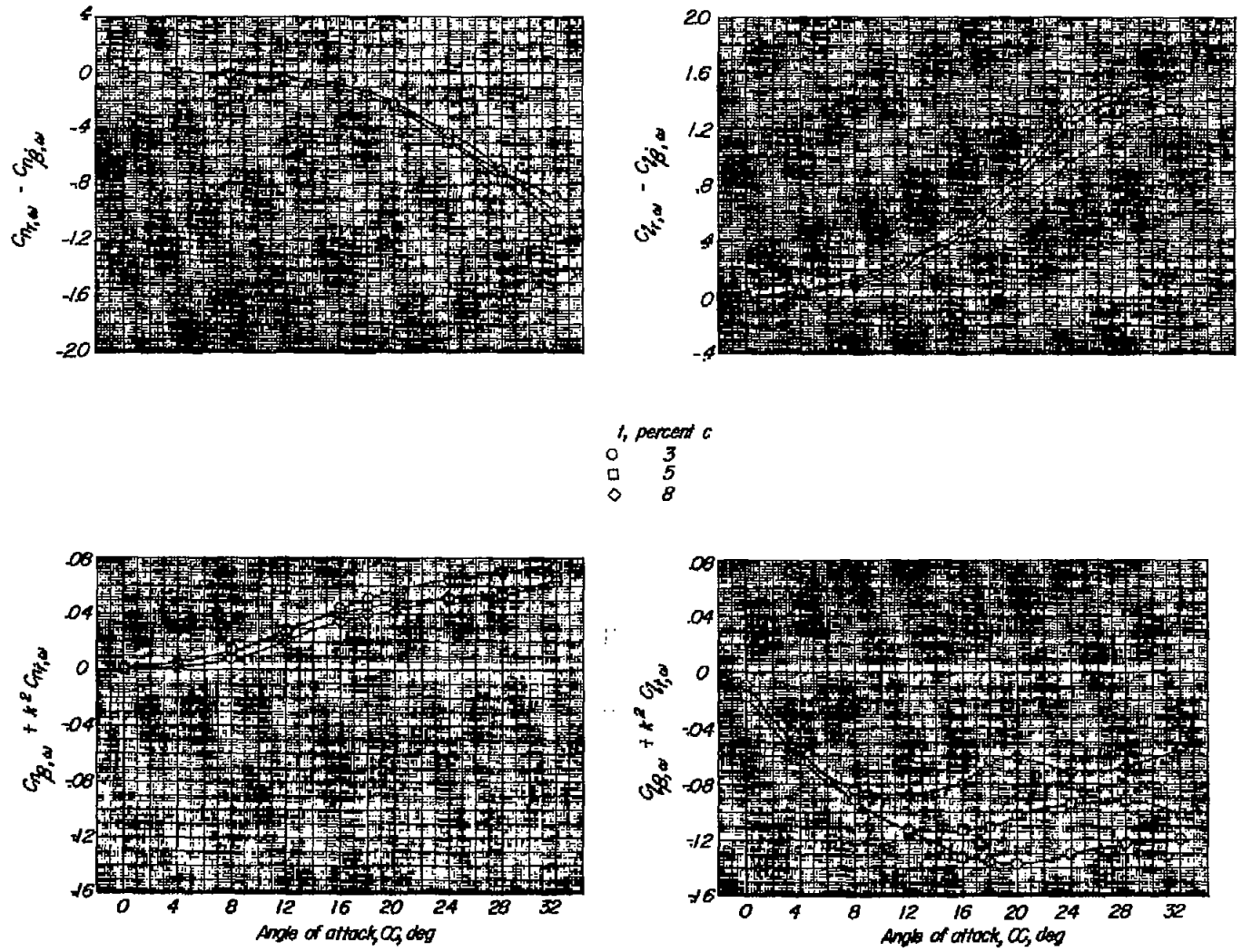

Figure 23.- Effect of profile thickness on the oscillatory stability derivatives for a 60° delta wing with a leading-edge radius of 0.791 percent c. $\psi_o = \pm 6°$; k = 0.132.

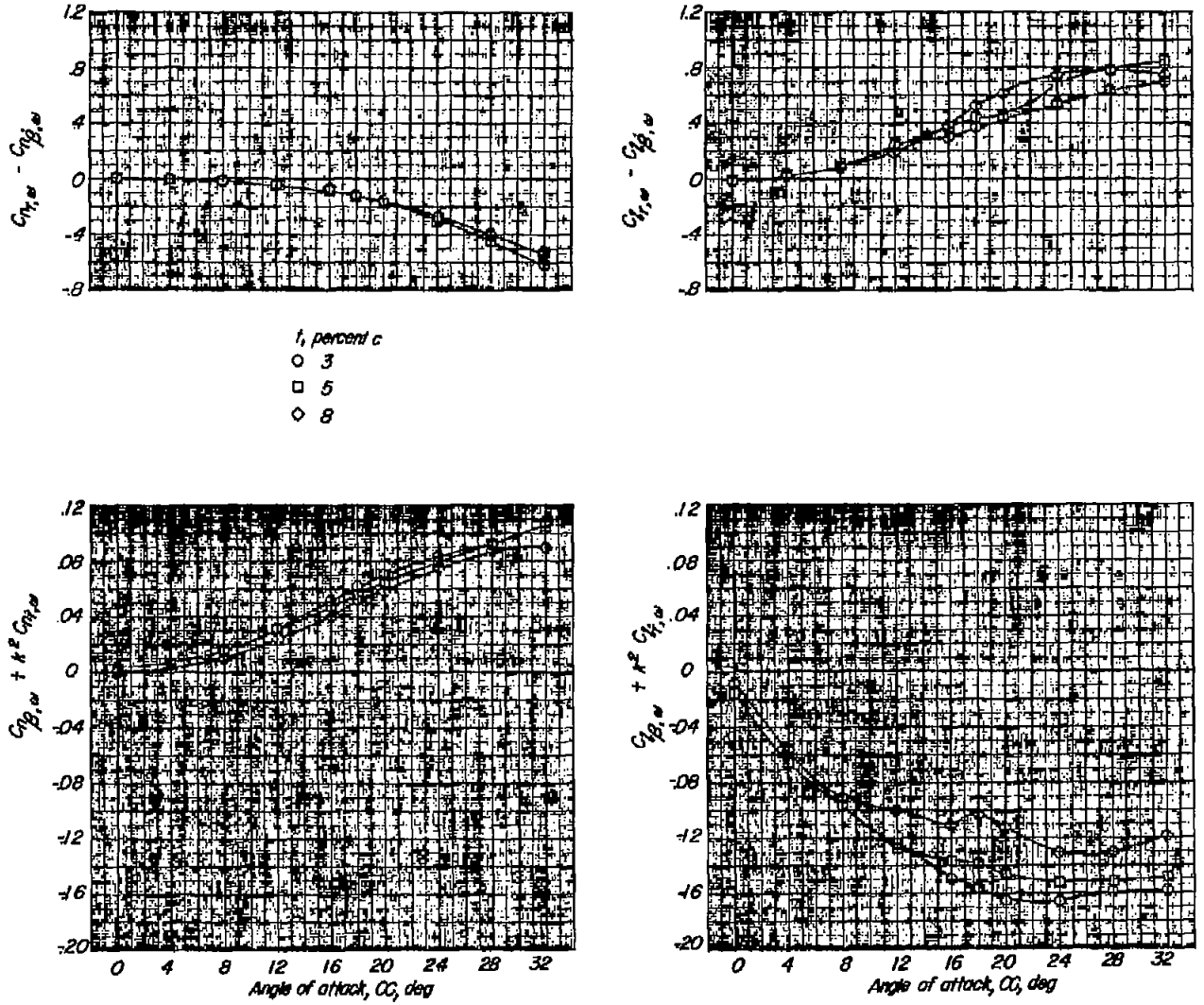

Figure 24.- Effect of profile thickness on the oscillatory stability derivatives for a 60° delta wing with a leading-edge radius of 0.791 percent c. $\psi_o = \pm 6°$; k = 0.218.

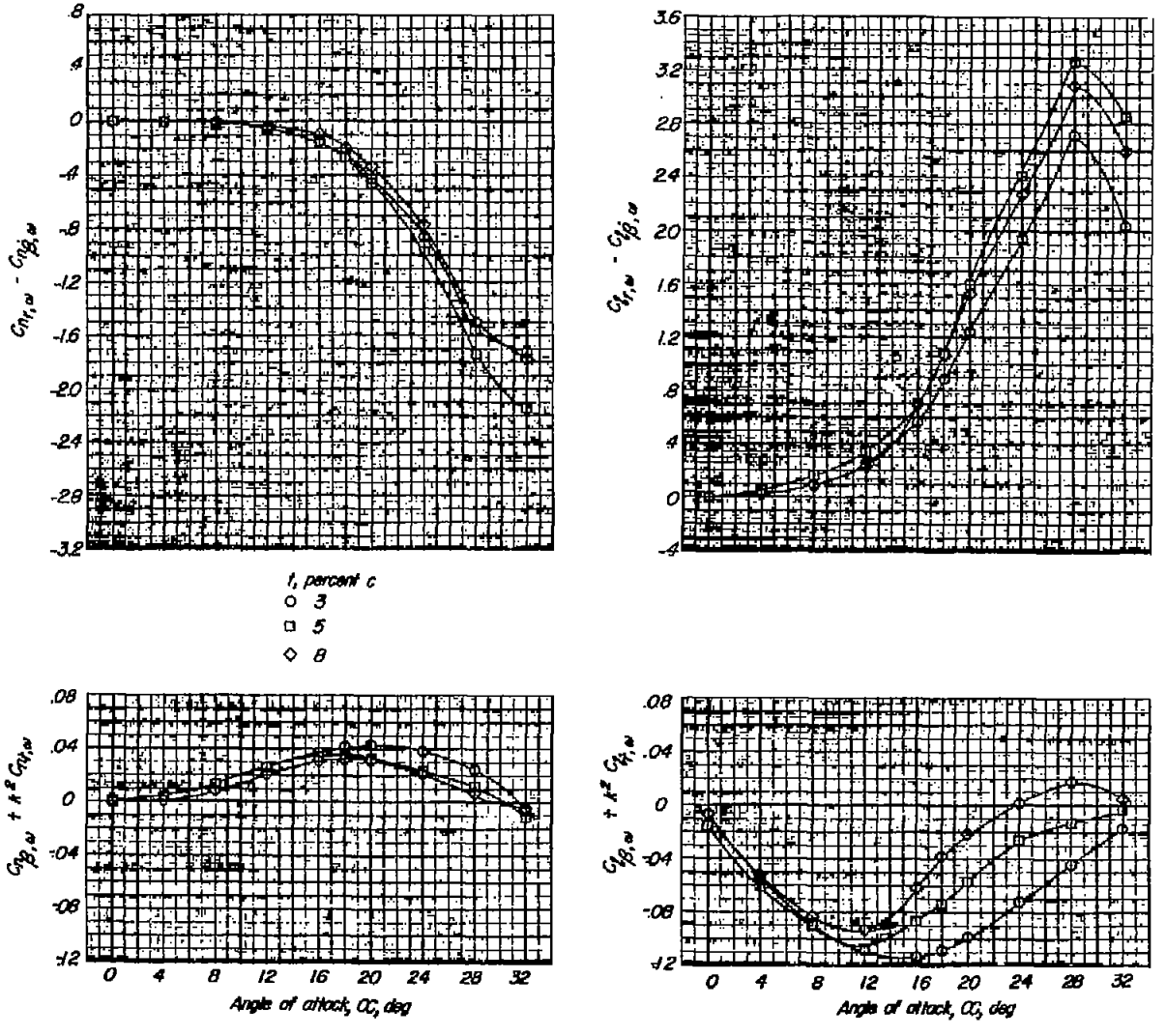

Figure 25.- Effect of profile thickness on the oscillatory stability derivatives for a 60° delta wing with a leading-edge radius of 0.791 percent c. $\psi_o = \pm 10°$; k = 0.066.

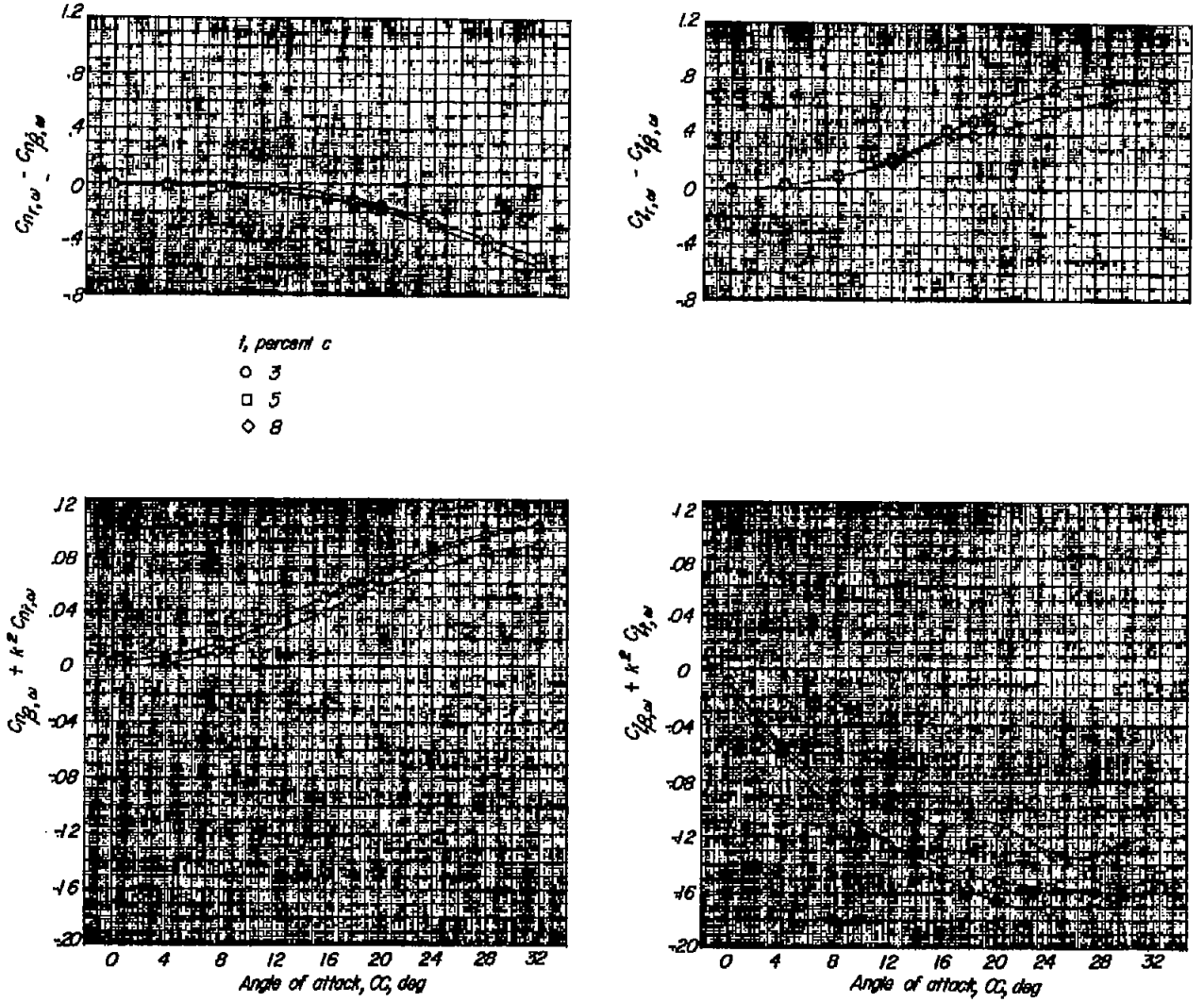

Figure 26.- Effect of profile thickness on the oscillatory stability derivatives for a 60° delta wing with a leading-edge radius of 0.791 percent c. $\Psi_o = \pm 10°$; k = 0.218.

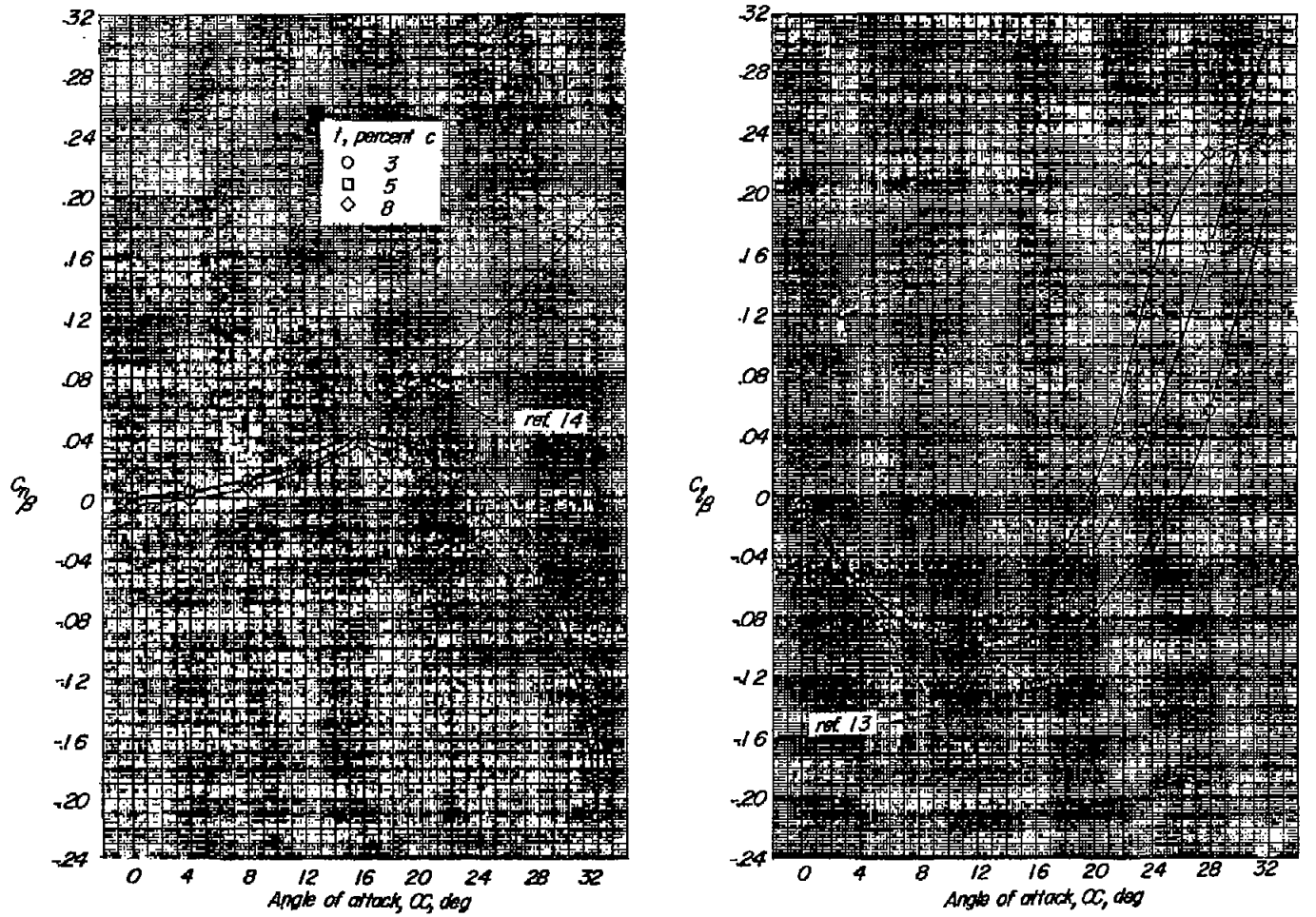

(a) $\psi_o = \pm 2^o$.

Figure 27.- Effect of profile thickness on the static stability derivatives for a 60° delta wing with a leading-edge radius of 0.791 percent c.

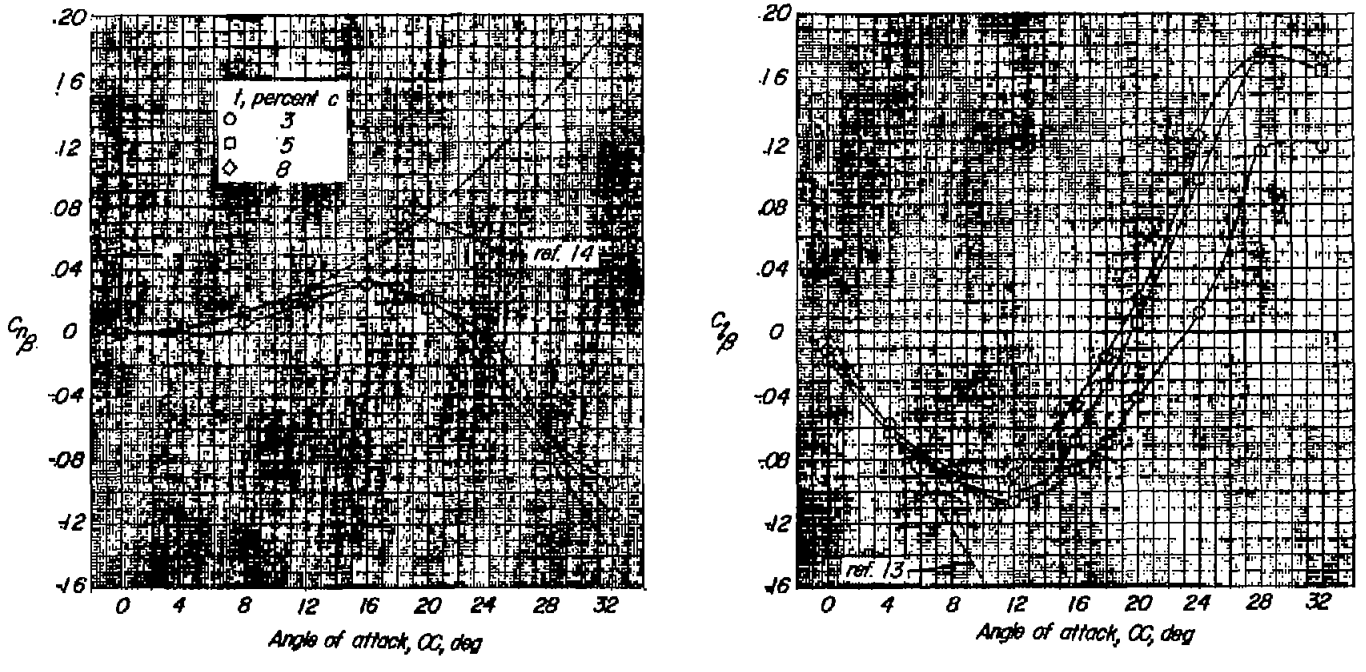

(b) $\Psi_o = \pm 6^o$.

Figure 27.- Concluded.

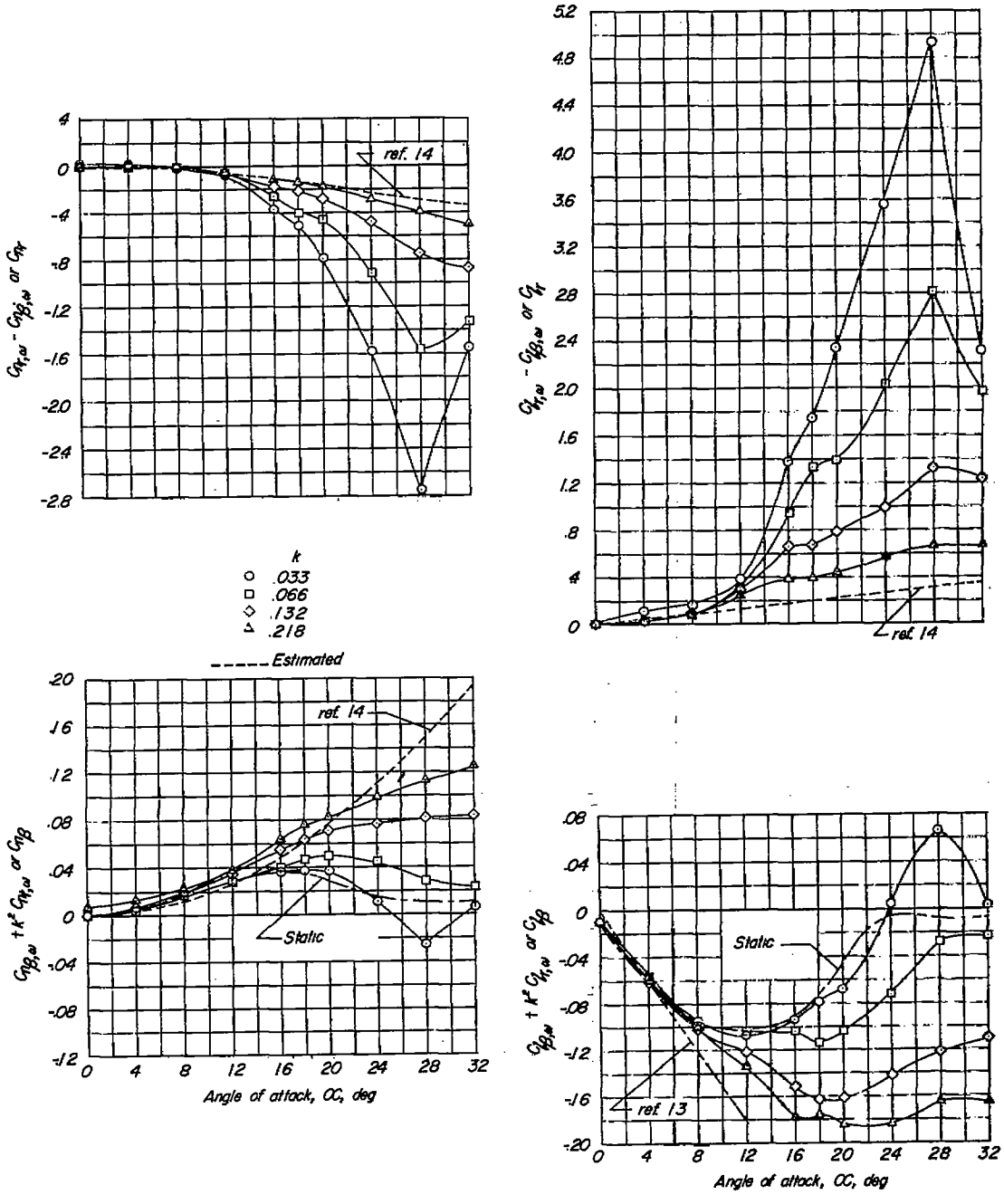

Figure 28.- Typical oscillatory stability derivatives for the 60° delta wing. L. E. radius = 0; t = 3 percent c; $\psi_o = \pm 6°$. Measured static values and estimated steady-state values are also shown.

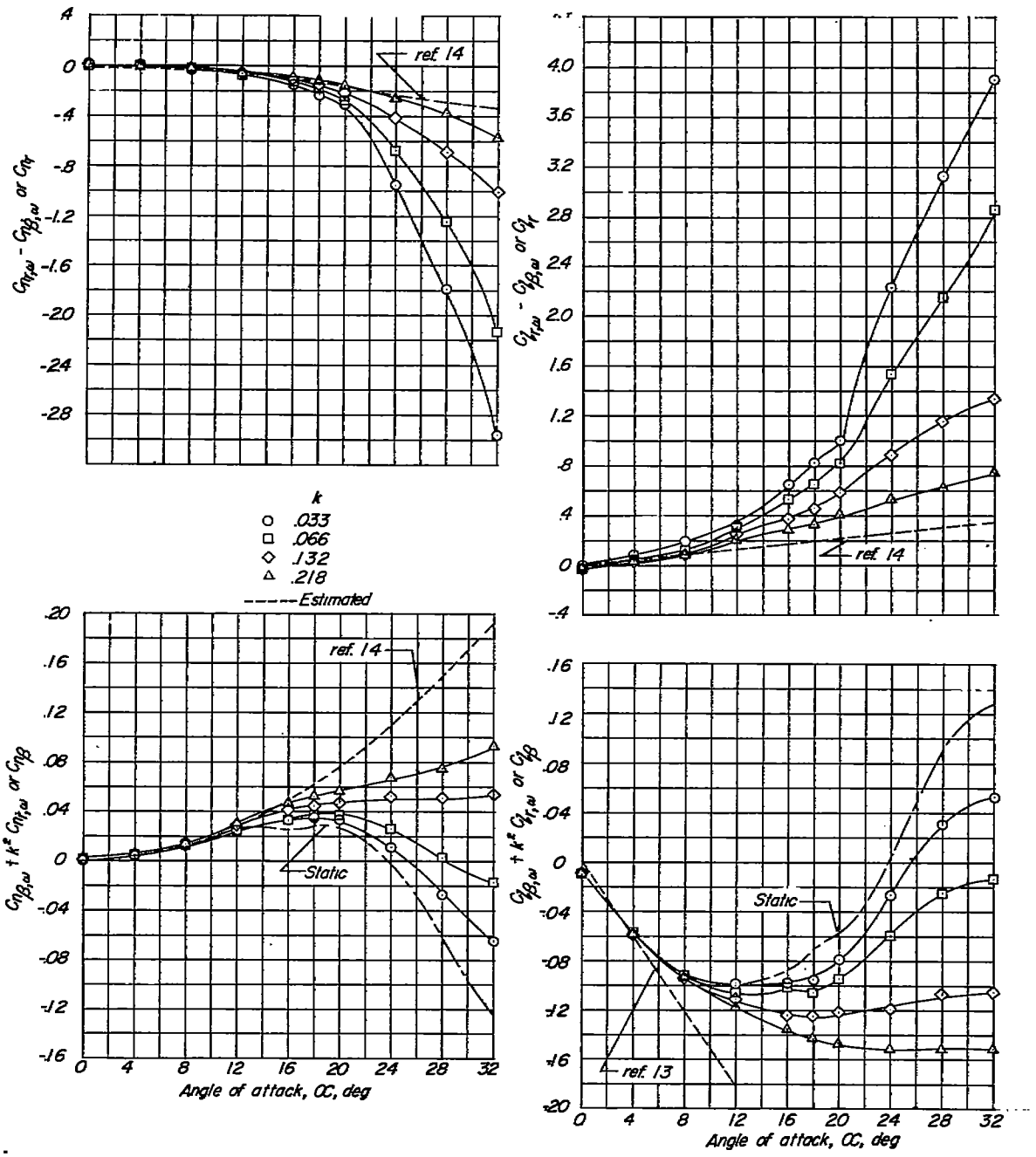

Figure 29.- Typical oscillatory stability derivatives for a 60° delta wing. L. E. radius = 1.582 percent c; t = 3 percent c; $\psi_o = \pm 6°$. Measured static values and estimated steady-state values are also shown.